Understanding cellular and behavioral consequences of Scn2a haploinsufficiency in cerebellar circuits

by
Chenyu Wang

DISSERTATION
Submitted in partial satisfaction of the requirements for degree of
DOCTOR OF PHILOSOPHY

in

Neuroscience

in the

GRADUATE DIVISION
of the
UNIVERSITY OF CALIFORNIA, SAN FRANCISCO

Approved:

DocuSigned by:
4AF406E430B7472...
Massimo Scanziani
Chair

DocuSigned by:
Alexandra Nelson
Alexandra Nelson

DocuSigned by:
Felice A. Dunn
Felice A. Dunn

DocuSigned by:
Kevin Bender
A996F2A5C1214BE...
Kevin Bender

Committee Members

Acknowledgements

I would like to thank my thesis committee members: Massimo Scanziani, Alexandra Nelson, Felice Dunn, and Kevin Bender for their valuable input throughout this entire project. I would also like to specially thank Kevin Bender and Guy Bouvier for their intellectual guidance on this thesis work. This project would not have been possible without their involvement.

The Bender lab at UCSF has provided an overwhelmingly supportive environment that made my graduate training a very memorable and enjoyable experience.

In addition, I want to thank the neuroscience graduation program at UCSF for all the support they provided, especially the program administrators Pat Veitch and Lucita Nacionales who have made my time in the program a very smooth journey.

Last but not least, I'm very grateful for the support and the community established by the FamilieSCN2A Foundation. It's the families and professionals who provided the motivation that ultimately drove this project forward.

Understanding cellular and behavioral consequences of *Scn2a* haploinsufficiency in cerebellar circuits

Chenyu Wang

Abstract

Ever since Hodgkin and Huxley described the sodium ionic current dependence in action potential nearly 70 years ago, neuroscientists have discovered an entire family of voltage-gated sodium channels (Na_Vs) in neuronal cells. Uncovering the differential distributions of these Na_V isoforms between and within each type of neuron has helped us understand the distinct roles they play in cellular functions. So crucial to normal neuronal physiology, genetic variants that result in protein structure changes can cause pronounced alteration in brain function and lead to diseases. $Na_V1.2$, encoded by *SCN2A*, is one Na_V isoform of which genetic variants have been linked to neurodevelopmental disorders such as autism spectrum disorder (ASD). Studies have uncovered the importance of $Na_V1.2$ in neuronal intrinsic properties and synaptic physiology in the forebrain along with their behavioral relevance. However, how these channels maintain normal cellular functions in the cerebellum, in which some of the strongest expression of $Na_V1.2$ are detected, is still unclear. The cerebellum is heavily implicated in ASD due to its functions in motor learning, fine movement control, and more recently discovered, cognition. Therefore, understanding how *SCN2A* dysfunctions alter cerebellar circuit has become critical to study disease manifestation in channelopathies. In my thesis work, I found that *Scn2a* haploinsufficiency in mice decreased cerebellar granule cell excitability, impaired high-frequency action potential propagation along their axons, and ultimately

compromised the downstream synaptic plasticity that is critical to cerebellar learning. I also used cerebellum-dependent vestibulo-ocular reflex (VOR) to uncover that mice with *Scn2a* heterozygosity exhibited saturated VOR gain and deficit in VOR adaptation, which are correlated with abnormal Purkinje cell activity pattern during behavior. In addition, children with LoF *SCN2A* variants showed a similarly elevated baseline VOR gain. Lastly, I revealed that the VOR adaptation deficit in mice can be rescued by upregulating *Scn2a* in the entire mouse brain using a novel CRISPR activation technique. I hope this work will contribute to our understanding of sodium channel function in the cerebellum and ASD.

Table of Contents

List of Figures

List of Abbreviations

AP: Action potential

ASD: Autism spectrum disorder

CRISPR: Clustered regularly interspaced short palindromic repeats

GC: Granule cell

LoF: Loss-of-function

LTD: Long-term depression (neurophysiology)

LTP: Long-term potentiation

Na_V: Voltage-gated sodium channel

PC: Purkinje cell

Pf: Parallel fiber

SCN2A or *Scn2a*: Human or mouse gene that encodes for $Na_V1.2$

VOR: Vestibulo-ocular reflex

General Introduction

To this day, neurons are considered the fundamental units of consciousness. Santiago Ramón y Cajal's neuron doctrine ignited an explosion of excitement that inspired century-long research on the functions and the dysfunctions of these specialized cells, which is still going strong today. Neurons, regardless of residing in the central nervous system or the peripheral segments, are connected through either gap junctions or chemical synapses[1]. They process information and communicate with other neurons via electrogenic activities that are generated by both active and passive exchanges of ions across the neuronal membrane[2]. The resting potential of the membrane is generally hyperpolarized around -70 mV due to the high intracellular potassium concentration that drives a negative membrane potential[2]. The information is encoded as phasic and sudden depolarizations called action potentials (APs), which are initiated by the opening of the voltage-gated sodium channels (Na_V)[2]. A large amount of Na ions rushes into the local intracellular space in as short as 1 ms and brings the membrane potential above 0 mV, which is termed the rising phase. This rising phase corresponds to the opening of the Na_Vs, which is one of the three states of Na_Vs. Immediately after, the depolarized membrane potential drives Na_Vs into their second state called inactivation. While the Na_Vs are inactivated, voltage-gated potassium channels open to allow efflux of potassium ions that quickly hyperpolarizes the membrane potential back to near resting potential, which releases Na_Vs inactivation and returns them to the closed state[3]. The duration of each neuronal AP can be anywhere between 2 to 5 ms, and the Na_Vs cycle through these three states for each AP. In unmyelinated neurons, the availability of Na_Vs on the membrane becomes crucial as AP propagates by triggering this type of active membrane

conductance along the entire axon until it reaches the end of the processes. This is especially true if a neuron presents an activity pattern that comprises series of high frequency APs. When there is a very short inter-AP interval, one can imagine that not all Na_Vs that were open from the previous AP have recovered from inactivation and are ready to open again. Therefore, having abundant membrane Na_Vs is crucial to sustain fast AP trains.

Different Na_V isoforms have been discovered in the mammalian systems, which differ from each other by expressing different α or β subunit variants[4,5]. These variations in Na_V subunits, especially in the α subunits, give rise to distinct properties of each isoform, including inactivation speed, voltage threshold, and ion selectivity[5]. Thus, the differential distribution of the Na_V isoforms in the central nervous system (CNS) allows various neuronal types to have their signature electric activity patterns. One of these Na_V isoforms, termed $Na_V1.2$, has broad expressions in the mammalian brains, including a large proportion of glutamatergic neurons such as cortical pyramidal cells and granule cells in the cerebellum[6–8]. In myelinated neurons where saltatory conductance is possible, $Na_V1.2$ have been found to be concentrated at the proximal site of the axon initial segment (AIS) to assist with AP backpropagation as well as in the dendrites where $Na_V1.2$ is believed to play a crucial role in facilitating dendritic integration[5,8–10]. The functions of $Na_V1.2$ in the distal axons of these neurons have been largely omitted as only $Na_V1.6$ are found at the Nodes of Ranvier – the active AP generation zones between myelination segments where mainly comprise of $Na_V1.6$[5]. Nevertheless, besides these long projection neurons, a large number of neuronal types in the brain is not myelinated, in which $Na_V1.2$ are expressed. Therefore, it is unclear how $Na_V1.2$ independently contribute to AP

propagation and the fidelity of these APs in the unmyelinated axons. The granule cells in the cerebellum provide an extraordinary platform to address this gap for several reasons. Not only are the granule cells the only glutamatergic excitatory neurons in the cerebellar cortex, but they are also the only neurons that express $Na_V1.2$[7,8]. In addition, the axons of these neurons are well-organized long projections that are neatly packed in the molecular layer of the cerebellar cortex, which makes it easy to localize and isolate them for experiments. More importantly, cerebellar granule cells generate APs in a bursting pattern–intermittent short AP trains with an extremely high average instantaneous frequency that can reach up to 1 kHz and an average at around 170 Hz[11–13]. One may hypothesize that having abundant Na_Vs is critical to these cells' ability to generate and sustain such fast mechanism of AP transduction.

Ultimately, the fidelity of the APs directly translates to the fidelity of the transmission onto the downstream neurons[14,15]. Chemical synaptic transmission requires neurotransmitter release from the presynaptic terminal and activation of the corresponding postsynaptic receptors. The machinery of neurotransmitter vesicles fusion is predominantly dependent on calcium binding to the synaptotagmin subdomains[16]. The major source of calcium at the axonal terminal is in the extracellular space, which is controlled by the opening of voltage-gated calcium channels that is triggered by APs. Since the trigger of each vesicle release is corresponding to the fourth order of calcium binding, meaning that four calcium ions are required for the exocytosis of each vesicle, this particularly non-linear relationship might increase the sensitivity to the accuracy of presynaptic activity that the release mechanism relies on[17].

The synaptic transmission can lead to both short-term and long-term changes at the postsynaptic site. In excitatory synapses such as glutamatergic synapse between granule cells and Purkinje cells, upon the activation of ionotropic glutamate receptor such as the α-amino-3-hydroxy-5-methyl-4-isoxazoleproprionic acid (AMPA) receptors, the opening of cation channels allows the influx of positively charged ions that generates excitatory postsynaptic current (EPSC), which leads to depolarization of the membrane, termed excitatory postsynaptic potential (EPSP)[18]. Long-term alterations at the synapse can result in changes in the strength of the transmission in both presynaptic and postsynaptic sites.

Further depolarization caused by temporal or spatial summations of presynaptic inputs can result in long-term alteration in the sensitivity of the postsynaptic membrane to presynaptic input due to ionotropic receptor insertion, resulting in larger EPSC from the same amount of glutamate being released, or long-term potentiation (LTP). On the other hand, desynchronized inputs can lead to a weakening of the synaptic strength that reduces the EPSC generated, or long-term depression (LTD)[18,19]. In addition, the synaptic strength can be a result of presynaptic alterations such as an increase or decrease of the probability of neurotransmitter release. However, the massive heterogeneity of induction and expression mechanisms of LTP and LTD across the brain eliminates the possibility of using only one generic model to describe all of them. For instance, although it is rare that both LTP and LTD can be expressed at the same synapse where both pre- and post-synaptic mechanisms can occur, the granule cell to Purkinje cell synapse in the cerebellum, however, is one of the locations that all four types of plasticity have been described[20–26].

In 1982, Ito and Kano first demonstrated that the excitatory input from granule cells to Purkinje cell was reduced by simultaneously stimulating granule cell parallel fibers and climbing fibers projected from the inferior olive nuclei (IO)[25]. This calcium dependent post-synaptic LTD was held as the only cerebellar learning model until presynaptic adenylate cyclase- (AC) and cyclic AMP (cAMP)-mediated LTP was described[20]. Soon after, it was shown that presynaptic LTD and postsynaptic LTP are both possible[23,24,27,28].

Regardless of the mechanism of these synaptic strength changes, the resultant effect on the postsynaptic cell remains the most meaningful component as it is one step closer to the eventual neural output that governs behaviors. The brain region that these granule cells resides in – the cerebellum – is possibly one of the most plastic and fastest computing regions in the brain. Thus, it has been known to be responsible for fine motor control, balance, gait, and motor learning, all of which require immediate feedback to environmental stimulus and instant error correction to prevent potential injuries[29–31]. As one of the most evolutionarily conserved brain regions, the cerebellum comprises of uniform and seemingly homogeneous circuits and cytostructural organizations. The cerebellar cortex is divided into three layers. The granule cell layer contains billions of granule cells somas that outnumber all the neurons in the entire brain. It is estimated that as many as three quarters of neurons in the brain are granule cells. Being the smallest neurons in the brain, their 4 μm-diameter somas allow these cells to be densely packed together[32,33]. Interestingly, these small neurons extend their axons into the molecular layer and bifurcate into parallel fibers that project along the molecular layer and contact the dendrites of the second largest neurons in the brain: Purkinje cells. Averaging at about 20 μm in diameter, their large soma size allows these neuron to form their own Purkinje

cell layer. Not only do they have large cell bodies, but they also have one of the largest dendritic arbors that extend to the length of the entire molecular layer. This allows each Purkinje cell to form hundreds of synaptic contacts with parallel fibers and integrate these inputs from many granule cells.

Decades of studies in non-human animal models have demonstrated the importance of parallel fiber to Purkinje cell synapse for underlying various types of motor learning[29,34]. Furthermore, research in mice has recently uncovered the role of the cerebellum in cognitive processing[31]. Despite the broadly used behavioral tasks designed for mice, human and mouse are fundamentally different species so that only limited interpretations can be made for observations in complex mouse behaviors. Fortunately, there are evolutionarily conserved cerebellum-modulated reflexes that are both functionally similar and can be simply quantifiable in human and mouse. Vestibulo-ocular reflex (VOR) is a form of oculo-motor reflexes that has strong dependence on the cerebellar circuit[35]. The main function of VOR is to stabilize the visual field at the center of the retina during body and head movement. As the name suggests, the motion is sensed by the semicircular canals that are an integral part of the vestibular system, which relays the afferent copy to the vestibular nuclei in the brainstem that control the ocular motor neurons to generate contraversive eye movement[36]. For instance, a clockwise head rotation will result in contraction of the temporal extraocular muscle of the left eye and the nasal extraocular muscle of the right eye, which, altogether, produces a counterclockwise movement of both eyes. Although the cerebellum is not required for this behavior, it actively modulates the amplitude of the eye movement given a certain degrees of head rotation. This is termed VOR gain. Besides the vestibular nuclei, a

sensory copy is also received by granule cells via mossy fibers. As the sole output neurons from the cerebellar cortex, Purkinje cells' GABAergic inhibitory output then relays back to the vestibular nuclei. Specifically, the floccular complexes is responsible for directly modulating eye reflexes such as VOR. Causal relationships have been demonstrated by optogenetically stimulating the flocculus on one side and successfully inducing ipsilateral eye movement in mice[37]. This strong evidence suggests that although the cerebellum is not required for VOR, its output is sufficient to manipulate ocular movement. The cerebellar circuit acts as a parallel tuning device that can turn VOR gain up and down. This type of tuning, or adaptation, is a form of cerebellar learning. Although VOR is defined as the involuntary eye movement generated by head motion, which is measured in the dark, VOR adaptation requires the pairing of visual input such as one that generates optokinetic reflex (OKR). Just like us, mice can also utilize these two complementary ocular reflexes to stabilize their visual field and navigate through their environment. In fact, multiple parallel lines of evidence have revealed that their ability to adapt VOR gain is strongly dependent on the plasticity at the parallel fiber to Purkinje cell synapse in the cerebellum[34,37–41]. However, these studies have primarily focused on synaptic proteins such as protein kinase C (PKC), cyclic GMP (cGMP), and the Ca/Calmodulin-dependent protein kinase (CAMK) family that are parts of the synaptic signaling pathway for plasticity induction in the Purkinje cells[38–41]. However, it is unclear how ion channels, such as $Na_V1.2$ that are expressed throughout the entire granule cell processes, may affect VOR.

$Na_V1.2$ is encoded by the *SCN2A* gene[42]. Recent large-scale exome sequencing studies have revealed a strong association of variants of sodium channel-encoding gene

SCN2A with many developmental disorders, including autism spectrum disorder (ASD)[43–45]. Gain-of-function (GoF) mutations of the *SCN2A* gene usually lead to epileptic encephalopathy or benign infantile familial seizures. On the other hand, Loss-of-function variants of *SCN2A* that result in either decreased Na$_V$1.2 activity or non-conducting channels can cause ASD or intellectual disability[42,46]. In addition, comorbidities such as gastrointestinal issues and sensory hypersensitivity are also common in *SCN2A*-related disorders, which can further worsen the debilitating conditions that those who are affected already experience[42]. Many recent studies have uncovered cellular and synaptic changes induced by loss of *Scn2a* in mice, which we might be able to utilize to infer how various *SCN2A* disorders manifest in humans[8–10,47]. Nevertheless, it is rather difficult to make any direct comparison between mouse behavioral phenotypes and disease symptoms in humans. Luckily, simple reflexes such as VOR offer the ability to extrapolate the translatability from the model organisms of interest to human. Moreover, the advantage of adopting this type of quantitative measurement is that it might have the ability to provide as an alternative clinical tool to assist with a more comprehensive diagnosis for ASD or neurodevelopmental disorders in general.

In my thesis work, I sought to address four major questions:

1. How does partial loss of Na$_V$1.2 affect cellular and synaptic physiology in the mouse cerebellar cortex?
2. How will altered neuronal physiology impact cerebellum-dependent behaviors such as VOR?

3. Will it be possible to reverse the behavioral deficit by rescuing $Na_V1.2$ expression in mouse?
4. Can we make the same observation in children with LoF *SCN2A* variants?

In this three-chapter dissertation, I will provide more relevant background knowledge in details, explanations on experimental design and setup, discussion on the data and potential interpretation on these results.

CHAPTER 1: *Scn2a* haploinsufficiency disrupts cellular and synaptic physiology in the mouse cerebellum.

Introduction

Whole exome sequencing studies have identified various genetic *de novo* mutations that contribute to autism spectrum disorder (ASD)[43–45,48]. In particular, *SCN2A* is one of the top high-risk genes for which the mutations are strongly associated with ASD[44,49–53]. *SCN2A* gene encodes for $Na_V1.2$, a subtype of voltage-gated sodium channel that is essential in neuronal function such as action potential (AP) initiation and propagation[9,54]. ASD patients with identified *SCN2A* variants usually present symptoms such as delay in development of language skills, social impairments and episodic ataxia, resembling the phenotype of those with cerebellar disorders[31,42,55–57]. Anatomically, age and sex matched postmortem tissues from ASD patients show abnormal cerebellar volume as well as reductions in Purkinje cell count and cell size[55,58–61].

The cerebellum governs precise movement, gait and postural control[29,30]. Human studies have reported that some patients with cerebellar lesions present autism-like symptoms such as self-stimulation behaviors, tactile defensiveness, ataxia, hypotonia, and sensory overload[31,56,57]. Moreover, it has been reported that both ASD and cerebellar lesion patients have oculomotor deficits in smooth pursuit, nystagmus, and vestibulo-ocular reflex (VOR)[56,62,63]. Indeed, the cerebellum gates motor learning during both early development and adulthood, including regulating both VOR and OKR, two cerebellar dependent innate reflexive behaviors that are well characterized in plasticity studies and

require long-term plasticity induction at the parallel fiber to Purkinje cell synapse[29,34,37–41,64,65].

$Na_V1.2$ channels are predominantly expressed in granule cells and the molecular layer but not in Purkinje cells, which is confirmed by both published data and our *Scn2a* promoter driven GFP expression (Fig. 1.1B, C)[8]. Being the only glutamatergic cell type in cerebellar cortex that are known for having bursting AP activity, loss of $Na_V1.2$ channel function will likely disrupt the ability of granule cells to accurately relay sensory information to downstream key synapses[11,13,34]. Along the axon, Na_Vs mediate the rising phase of an action potential, entering an inactivation state that does not allow immediate reopening of the channel[2,3,66]. Therefore, a decreased availability of $Na_V1.2$ in *Scn2a* haploinsufficiency condition may impair the ability of sustaining a high frequency activity pattern, or bursting, in granule cells. As AP failure is a likely consequence of *Scn2a* haploinsufficiency, the waveform of single action potentials under high frequency stimulation can also be altered while propagating along the parallel fibers. The lack of $Na_V1.2$ reduces inward current mediated by Na ions that leads to a decreased driving force for potassium outward current, which will likely cause a slow decay of the action potential. In addition, AP failure, AP waveform change, or both, may alter calcium-mediated neurotransmitter release at their synapses to Purkinje cells, as neurotransmitter release is nonlinearly dependent on Ca influx, small changes in Ca influx—driven by altered APs—can lead to pronounced changes in vesicle release kinetics at axonal terminals[17,67,68].

It has been reported that the duration of each AP train, or the number of APs, in the parallel fibers can lead to differential induction of long-term plasticity in the post-synaptic Purkinje cells[28,69]. This suggests that insufficient $Na_V1.2$ expression can directly

disrupt normal synaptic plasticity as partially blocking Na_Vs has been found to alter synaptic depression[70]. This is especially applicable to the activity patterns in the granule cells as $Na_V1.2$ availability is crucial to sustain these rapid bursts in unmyelinated axons. This very synapse holds an extraordinary level of complexity. Both LTP and LTD have been shown to be inducible at the presynaptic or postsynaptic site, that is, the parallel fiber terminal or the Purkinje cell, respectively. Unlike the canonical understanding of the calcium dependence in the hippocampus where high concentration of calcium in CA1 pyramidal neurons results in synaptic potentiation, the plasticity rule in the Purkinje cells is found to be reversed. For presynaptic-induced plasticity, the activation of the AC to cAMP signaling pathway governs the LTP, whilst the retrograde release of endocannabinoid and activation of endocannabinoid receptor lead to a decrease in probability of neurotransmitter release and results in LTD[20,22]. In contrast, nitric oxide is sufficient to induce postsynaptic LTP and large influx of calcium by co-activating both parallel and climbing fibers lead to prominent LTD[23,25]. The diversity of plasticity induction mechanisms enables the unprecedented flexibility in each direction in which the strength of parallel fiber input can be tuned. Nevertheless, it is not immediately clear how loss of $Na_V1.2$ can indirectly impact the activation of these individual pathways and results in altered plasticity. Altogether, the question of how *Scn2a* haploinsufficiency can impair the intrinsic excitability of the granule cells, AP propagation properties, as well as the synaptic plasticity needs to be addressed.

Results and interpretation

Early works have shown that density and availability of Na_Vs are crucial for both generation and propagation of action potentials, especially in unmyelinated axons such as granule cell parallel fibers where AP propagation relies heavily on continuous active membrane conductance[71,72]. Our patch clamp recording in cerebellar granule cells shows that a reduction in $Na_V1.2$ availability caused a decrease in the peak dV/dt and excitability (Fig. 1.1E). An elevated threshold for AP generation will likely affect how granule cells integrate mossy fiber inputs under *Scn2a*$^{+/-}$ condition, which can disrupt normal cerebellar function. This change was not observed in Purkinje cells, in which $Na_V1.2$ are not expressed in (Fig. 1.1F).

In addition, high frequency bursting activity of the granule cells requires sufficient Na_Vs to ensure reliable AP propagation. The number and density of available Na_Vs become more crucial in these unmyelinated axons where saltatory conductance is not possible. To test whether the reduction in $Na_V1.2$ availability impacts AP propagation in the parallel fibers, I evoked extracellular axonal-generated fiber volleys (FVs) and recorded their propagation from 1 mm away in the same molecular layer (Fig. 1.1A). *In vivo* whole-cell patch clamp recordings in mice have shown that these granule cells have average AP burst frequency around 170 Hz[11]. Therefore, I used a 166 Hz stimulating frequency with 20 stimuli per train to mimic physiological conditions. I also used a lower frequency protocol at 50 Hz to examine AP propagation properties. The fiber volleys showed *Scn2a* haploinsufficiency impaired the ability of these axons to sustain long-duration AP train at high frequency, evident by a significant reduction in their amplitudes (Fig. 1.1G). This was not observed at lower frequency (Fig. 1.1G). Moreover, it is also

noticeable that the last fiber volley is broadened when comparing to the first FV in *Scn2a* heterozygosity. The reduction in fiber volley amplitude suggests that there is AP propagation failure, whereas the waveform widening can suggest that there is a desynchronization of the AP propagation velocity. This result is consistent with a previous study where *Scn2a* heterozygosity caused AP waveform broadening in neocortical neurons[73].

It is well known that AP propagation can directly affect neurotransmitter release at the axonal terminal by directly changing calcium influx dynamic. AP generation and propagation impairment in granule cells and parallel fibers can ultimately lead to changes in synaptic transmission and even deficits in plasticity[14,15,70]. I tested whether the synaptic properties at the parallel fiber to Purkinje cell synapse are altered in *Scn2a* heterozygosity, I performed whole-cell voltage-clamp recordings in the Purkinje cells while delivering the field electric stimuli identical to what was used to evoke fiber volleys (Fig. 1.1A). Examining the excitatory postsynaptic currents (EPSCs) revealed that the total charge transfer decreased over the course of each stimulation train in *Scn2a*$^{+/-}$ mice, comparing to WT (Fig. 1.1H). These results demonstrated that *Scn2a* haploinsufficiency can alter short-term facilitation at this synapse.

As an extremely dynamic synapse, various forms of long-term plasticity have been uncovered, including pre- and post-synaptic long-term potentiation and pre- and post-synaptic long-term depression, all of which have been shown to be critical for cerebellum dependent learning[34,37–41]. Since the short-term facilitation is impaired in the *Scn2a*$^{+/-}$ mice, LTP should be too. To test whether LTP is impaired in *Scn2a* haploinsufficiency, we modified a high-frequency burst-dependent LTP induction protocol to mimic the

physiological pattern of *in vivo* bursting activity of granule cells[69]. In WT, LTP could be successfully induced, which is shown as an increase in EPSC amplitude (Fig. 1.1D). Nevertheless, the *Scn2a*$^{+/-}$ did not show any sign of LTP expression (Fig. 1.1D). This is somewhat consistent with our current understanding in the relationship between AP properties and synaptic physiology. There is sufficient evidence that show both AP failure and waveform change can cause reduction in calcium influx at the axonal terminals and, in turn, render plasticity induction unsuccessful[14,15,71]. In this experiment, I did not intentionally target any specific location for LTP expression. I recognize that the current induction method was modified from a post-synaptically expressed LTP protocol[69]; nevertheless, the fact that I could also observed a decrease in paired-pulse ratio (PPR) in neurons that successfully expressed LTP suggests a partial presynaptic probability of release increase during LTP induction. This can be due to a prolonged duration of each stimulus train, which might activate the cAMP to PKA pathway as previously reported[20].

In conclusion, I found that constitutive loss of $Na_V1.2$ in cerebellar granule cells noticeably reduced the intrinsic excitability of these neurons compared to WT, but these properties were intact in the Purkinje cells. Furthermore, parallel fibers with only half of $Na_V1.2$ expressed were not able to sustain high-frequency axonal-induced FVs. The observation of reduction in FV amplitude and the broadening of halfwidth might play a crucial role in leading to the LTP failure after burst-based induction.

CHAPTER 2: *Scn2a* haploinsufficiency alters cerebellum-modulated oculo-motor behavior.

Introduction

As I continued to explore how *Scn2a* dysfunction can impact cerebellar physiology, it is difficult not to think about how such a strong cellular and synaptic deficit might change cerebellum dependent behaviors. Many recent studies have pointed out the higher function modulations such as cognition and social behaviors that the cerebellum is responsible for[74–76]; however, its long-standing reputation in governing motor learning highlights the strong dependence on synaptic plasticity. The seemingly simple and uniform cytoarchitecture and circuitry have shifted the focus of decades of research away from it. Nevertheless, the complexity and apparent heterogeneity within the cerebellar cortical structure have proven the opposite, part of which might be due to the sheer number of granule cells, the only glutamatergic neurons in the cerebellar cortex that receive the afferent copy of the sensory input from mossy fibers, which makes up more than half of the neurons in the brain. Each granule cell and its axon is thought to be finetuned to a narrow range of sensory coding such as movement velocity or limb position[77,78]. With estimated 50 billion granule cells in the cerebellum, it is nearly impossible to dissect and map the function of each individual one of them. As I have shown earlier, *Scn2a* loss has raised the AP threshold and decreased the velocity of AP generation in granule cells, which, in turn, disrupts downstream synaptic plasticity. It is intuitive to hypothesize that these changes would alter behavioral phenotypes that are underlain by the cerebellar cortical circuitry.

Among all the cerebellum dependent behavioral tasks, oculo-motor reflexes are perhaps some of the most evolutionarily conserved, quantitative, and translatable behaviors that can be studied and compared directly between human and mouse. As we navigate through our daily lives, most of us rely heavily on our vision. Meanwhile, we set our body and head in a dynamic range of motion to assist with scanning our environment or identifying a visual target to either approach or avoid. By adopting this technique, there is one critical obstacle that our sensory system needs to overcome: an inevitable destabilization of our visual field during self-initiated movement. Thankfully, we subconsciously utilize visually and movement triggered eye reflex, termed optokinetic reflex (OKR) and vestibulo-ocular reflex (VOR), respectively, to counter any unwanted movement of the image on our retina. OKR describes an involuntary eye movement towards the direction of any moving object within our visual field, while VOR describes the eye movement in the opposite direction of our head motion[29,79,80]. These two reflexes usually function in concert to stabilize our gaze towards the same visual target.

The VOR circuit is rather simple and well-studied. Simply, the motion-sensing vestibular organs innervate the vestibular nuclei in the brainstem, which then control the downstream oculo-motor neurons to generate eye movement. The cerebellum provides a parallel circuit that receives the afferent sensory copy of the movement input and relays back to the vestibular nuclei to control the gain of the vestibular output. Although the cerebellar pathway is not required to generate VOR, it serves as a crucial tuning machinery to ensure the accuracy and precision of eye movement to optimally stabilize our vision. This type of tuning can be measured as the degree of the eye movement relative to the amplitude of the vestibular stimulus, termed gain, which is highly dependent

on the cerebellar plasticity. Parallel evidence has demonstrated that perturbing key elements in the parallel fiber to Purkinje cell synapse that are critical to plasticity balance disrupted VOR gain adaptation. Building upon the original Marr's theory of the cerebellum where long-term depression (LTD) in the Purkinje cell was initially thought to be the only crucial type of synaptic plasticity that allows for cerebellar learning[25,81], recent studies have revealed the expressions of LTP and LTD at both presynaptic and postsynaptic sites. Multiple lines of evidence have shown that manipulating granule cell to Purkinje cell synapse can directly disrupt VOR gain adaptation, suggesting this synapse is required for VOR gain modulation. The delicate and fluid balance of the potentiation and depression highlights the importance of a fully functional circuit. Previously, I have shown that the LTP in the cerebellar cortex is impaired in *Scn2a* haploinsufficent mice, but whether VOR plasticity is also compromised still remains to be tested.

Results and interpretation

To test this hypothesis, I used a custom-built experimental setup to record VOR in mice with *Scn2a* heterozygosity (Fig. 2.1A). In a simplified way, the setup consists of a motorized platform to provide rotational stimulus that generates compensatory eye movement, and an infrared (IR) light sensitive camera to capture the eye movement (Fig. 2.1A). By providing an oscillating rotation of which the angular velocity follows a sinusoidal pattern, I could generate a near-sinusoidal eye movement that is reversed in phase. Analyzing this type of eye movement revealed that the VOR gain in the *Scn2a*$^{+/-}$ mice is saturated near 1.0, comparing to much lower gains in the wild type littermates (Fig. 2.1B-D, Fig. 3.4C-E). As the VOR gain is sensitive to the temporal frequency, these mice were

also tested under different frequencies, during which they showed elevated gain as well (Fig. 3.4F). This observation seemed surprising at first, but a closer dissection of the cerebellar circuit provided a possible interpretation: loss of LTP at the parallel fiber to Purkinje cell synapses weakens the excitatory input onto the Purkinje cell, which releases the inhibition from PC to the brainstem nuclei, thus results in a near-unity VOR gain. If this theory is correct, then the plasticity-dependent VOR adaptation should also be affected in *Scn2a*$^{+/-}$ mice.

To induce change in VOR gain, I paired the oscillating rotation with a visual stimulus that moves in concert with the platform (Fig. 2.1A, middle). The visual stimulus serves as an OKR stimulus that minimalizes the VOR gain. The goal of this adaptation induction is to temporarily suppress VOR gain, hence termed, VOR gain-down. There are two reasons for choosing to test this type of adaptation over other induction protocols such as gain-up: 1) the VOR gain in *Scn2a*$^{+/-}$ mice is saturated at unity, it is crucial to test whether this is due to a lack of plasticity that rendered then unable to decrease their VOR gain; 2) it has been reported that gain-down adaptation might be a result of LTP at the parallel fiber to Purkinje cell synapse, which is the phenomenon that we observed in our ex vivo experiment from these *Scn2a*$^{+/-}$ mice. By comparing the VOR gain recorded from before (baseline) and immediately after (post) gain-down induction, it is clear that the induction protocol successfully suppressed VOR in the WT, but the VOR responses in the *Scn2a*$^{+/-}$ mice were unaffected (Fig. 2.1B-D). This result confirms that the aberrantly high VOR gain in the *Scn2a*$^{+/-}$ mice is insensitive to adaptation.

With only behavioral readout, it is perhaps easy to speculate but difficult to verify how, or if there is any, changes in the cerebellar physiology due to *Scn2a* loss during

baseline VOR and gain-down adaptation. For this reason, I also employed extracellular unit recording to identify potential difference in the output from the cerebellar cortex, specifically in the floccular complex that has been shown to influence eye movement (Fig. 1A, left). As the sole output neuron from the cerebellar cortex, Purkinje cell activity directly represents the modulation of the downstream structure. Interestingly, comparing between baseline and post-induction, the simple spike firing frequency of the Purkinje cells in the WT mice increased as the VOR gain went down (Fig. 2.1E, F). An elevated Purkinje cell activity could suggest that LTP at the parallel fiber to Purkinje cell synapse might be present due to VOR gain-down induction. In contrast, an unaltered VOR gain in the *Scn2a*$^{+/-}$ mice correlated with a reduction in the Purkinje cell simple spike firing frequency (Fig. 2.1E, F). I observed similar changes in simple spike firing frequency during induction where the separation of normalized firing rate in WT and *Scn2a*$^{+/-}$ mice started diverging after the first 5 minutes of induction (Fig. 2.1G). In order to draw the correlation between PC simple spike firing rate and reduction in VOR gain, I ensured that there was no variability between animals by taking the ratio of the change in VOR gain to the change in PC firing rate. A clear separation between WT and *Scn2a*$^{+/-}$ mice demonstrates that the results are consistent across different mice in each experimental group (Fig. 2.1H).

It has been very well reported that the activity of Purkinje cells in the floccular complex modulates VOR gain. Although it has been shown that knocking out P/Q type calcium channels at the axonal terminals of parallel fibers can impact glutamate release and leads to VOR deficit, many studies have introduced perturbations directly in the Purkinje cells to observe their effects on VOR adaptation[34,38–41].

Although decades of research have demonstrated clear causal relationship between cerebellar physiology and VOR, *Scn2a* expression is not exclusive to this brain region. A growing body of literature has revealed the impact of *Scn2a* dysfunction in the prefrontal cortex, hippocampus, and the striatum, which are critical structures that are important for cognition, memory, and motor control[9,82,83]. To rule out the possibility that our observation is affected by *Scn2a* loss in cortical regions, such as the visual cortex, I needed to test the same hypothesis in mice that carry *Scn2a* haploinsufficiency in only the cerebellum. By crossing an alpha6-cre driver line with another mouseline that has one conditional knockout allele (*Scn2a*$^{+/fl}$), I could create constitutive *Scn2a* loss mostly in cerebellar granule cells (Fig. 2.2A, left). After repeating the VOR induction experiment with simultaneous *in vivo* unit recordings, I found that mice with *Scn2a* haploinsufficiency only in granule cells exhibited the identical VOR phenotypes, including an elevated VOR gain during baseline and an inability to reduce the gain (Fig. 2.2B, C). Their Purkinje cell activity also matches with those with constitutive whole-brain *Scn2a* heterozygosity (Fig. 2.2E, F). These results confirm the specificity of the VOR deficit in cerebellar granule cells.

To further examine the region specificity of this effect, I directly injected Cre into the floccular complex on both sides of the cerebellum (Fig. 2.3A, B). Interestingly, acutely knocking out *Scn2a* in the floccular complex did not alter the baseline VOR gain, but disrupted VOR adaptation ability (Fig. 2.3C). There are two possible hypotheses that remain untested: 1) baseline VOR gain is modulated elsewhere in the cerebellum, and 2) baseline VOR gain is development dependent and is set during a critical window. Although not specific to *Scn2a*, studies have shown that silencing cerebellar regions

outside of the floccular complex did not affect VOR gain, which makes the first hypothesis unlikely. There are several experiments that can potentially address the second hypothesis. One straightforward approach is to perform the same bilateral Cre injections in the floccular complex in very young mice such as those postnatal day 0 to day 4. The caveat would be that the small brain size will limit the accuracy and precision of injection.

These data have demonstrated that *Scn2a* haploinsufficiency can significantly dampen VOR plasticity by directly altering cerebellar physiology, specifically at the parallel fiber to Purkinje cell synapses that have been shown to modulate VOR gain and other oculo-motor behaviors. Interestingly, while the *Scn2a*$^{+/-}$ mice exhibit an extremely high VOR gain, when measured in the darkness, their visually triggered reflex such as OKR, did not seem to be affected. During gain down induction, both WT and the *Scn2a*$^{+/-}$ mice showed near complete acute suppression of VOR when presented with a moving visual stimulus. Similarly, both groups showed identically elevated gains when the VOR was measured in a luminated condition (Fig. 2.4). The difference only became apparent after removing the visual stimulus.

In summary, I found that *Scn2a*$^{+/-}$ mice have a near unity baseline VOR gain and an inability to reduce their gain after they were subjected to a gain-down induction protocol. The Purkinje cell firing frequency in the floccular complex increased while the VOR gain decreased in WT; on the other hand, the PC firing frequency in *Scn2a*$^{+/-}$ mice decreased after gain-down induction. These results were consistently observed in a6Cre::*Scn2a*$^{+/fl}$ mice, in which *Scn2a* heterozygosity is constrained in the cerebellar granule cells. When *Scn2a* haploinsufficiency was introduced only in the floccular complex during adulthood, the mice showed a similar deficit in gain-down adaptation but

WT-like baseline VOR gains. No visual deficit was observed in any of the genetic manipulations and mouse groups. These data highlight specific cerebellar pathway that *Scn2a* dysfunctions might affect. Combined with the data shown from the previous section, this draws a full picture, from intrinsic cellular excitability to behavior, of how *Scn2a* related disorders, including ASD, manifest in the cerebellum.

CHAPTER 3: Examining the reversibility and translatability of oculo-motor deficit due to *Scn2a* haploinsufficiency.

Introduction

SCN2A-related disorders, including ASD, affect children at a very young age, many of whom are non-verbal[42]. Although it is difficult for us to know how much their perception is affected by the elevated VOR gain we see in *Scn2a* haploinsufficient mice, it can serve as a quantitative biomarker to assist with diagnosis or treatment efficacy evaluation. However, this raises the question of whether increasing *Scn2a* gene expression in adulthood can reverse VOR adaptation deficit to a WT level. To test this, I took advantage of an existing CRISPR activation (CRISPRa) approach. CRISPRa does not directly change the genetic sequence of the neurons. Instead, it works by activating the promoter of the gene of interest and overdriving the functional allele to elevate the expression level[84]. This prevents permanent gene editing that can potentially cause irreversible consequences that are often detrimental. Not only has CRISPRa been shown to be effective in reversing genetic disorder phenotypes[85], more importantly, it has been validated specifically for *Scn2a* gene and showed successful rescue of neuronal properties that were originally lost due to *Scn2a* dysfunctions[84].

Moreover, route of administration (ROA) should also be a consideration as it directly influences the efficacy of the CRISPRa construct, as well as the brain region of target. As a gene that is expressed throughout the brain, perhaps the most logical approach is to target the entire brain when considering the therapeutic benefits. This inevitably points to the direction of systemic administration as it might be difficult to reach

a large area through traditional transcranial infusion. Thankfully, a specific PhP.eb construct allows for crossing the blood-brain-barrier that clears the obstacle to deliver CRISPRa systemically. Previous work has shown that the construct infused from the mouse tail vein could successfully reach the prefrontal cortex and rescue neuronal properties[84]. However, the metabolism significantly lowered the efficacy of CRISPRa. Therefore, we identified that CRISPRa delivery through the retro-orbital (RO) sinus can bypass the majority of the metabolic process and enter the CNS directly from the cerebral-spinal fluid[86].

Developed by the Ahituv lab at UCSF, the injectable is consist of two separate AAV constructs (Fig. 3.1A). The first one contains an mCherry reporter sequence that will allow visual validation of the success of systemic delivery. The other construct contains the dCas9 construct either with *Scn2a* guide RNA (sgRNA) to target *Scn2a* expressing neurons, or without the sgRNA to serve as an empty vector control. This provides an exceptional tool to test if *Scn2a* expression in the brain is causal to VOR adaptation.

The ultimate goal of this thesis work is to hopefully contribute to the progress of identifying key mechanisms and advancing healthcare for those who are affected by ASD. Although the protein structure and function of $Na_V1.2$ is comparable between human and mouse, we cannot definitively conclude that children with *Scn2a* loss-of-function (LoF) variants, comparable to that of *Scn2a* haploinsufficiency, exhibit a similar behavioral phenomenon such as an VOR gain saturation. To address this, we developed an eye tracking device using a light-weight helmet with an attached IR-sensitive camera and a motion tracking device to record eye movement and head movement, respectively (Fig. 3.4A). As most of the children with *SCN2A* LoF variants are non-verbal and are not at

ease in novel environment, we did not want to keep the wearable on them for an extended period. Therefore, instead of testing whether the children were able to adapt to VOR gain-down plasticity, we decided to only assess their eye movement during baseline VOR, which requires them to tolerate the device for only one to two minutes. For the rotational stimulus to be as consistent with what we use in the mouse experiments, we employed a metronome to guide a manual oscillating rotation of the office chair while the child was sitting in it. Because recording VOR requires a completely dark environment, the experimenter who was in control of the chair was also equipped with a pair of night vision goggles to approximate the rotation amplitude to 5 degrees in each direction by following the preset markers on the floor. Since we recognize that manually controlled rotation lacks the absolute precision compared to a motorized stage we used in our mouse experiment, we can normalize the eye movement to the head rotation recorded by the motion tracking device to obtain a more accurate set of data.

Results and interpretation

After delivering the CRISPRa constructs through RO in the *Scn2a*$^{+/-}$ mice, they were given 30 days to allow for sufficient expression and upregulation of $Na_V1.2$ (Fig. 3.1A). These mice underwent the same VOR gain-down induction protocol with simultaneous *in vivo* unit recordings in the floccular complex. After the experiment, these mice were sacrificed, and their cerebellum were extracted for histological validation (Fig. 3.1B). Upon acute extraction, a small part of the cerebellum was sectioned off, immediately snap frozen in liquid nitrogen, and delivered for quantitative PCR to examine

Scn2a expression level. Coronal sections were made from the rest of the cerebellum and imaged for mCherry expression (Fig. 3.1B).

Five out of six *Scn2a*$^{+/-}$ mice that received CRISPRa showed restored ability to adapt to gain-down induction, evidenced by a significant reduction in VOR gain compared to *Scn2a*$^{+/-}$ mice that received the empty vector (Fig. 3.1D). Additionally, in the five mice that showed a behavioral rescue, the qPCR results also detected an increase in *Scn2a* mRNA expression level when normalized to the empty vector controls (Fig. 3.1C). This is very exciting as we were able to demonstrate that we can utilize systemic delivery approach to successfully restore gene expression that leads to behavioral rescue. Nevertheless, administering CRISPRa at P30 did not alter the baseline VOR gain to a WT level (Fig. 3.1D). This is the opposite but consistent with what I observed in mice injected with Cre in their floccular complex at P30 where their VOR adaptation was affected but not baseline VOR gain (Fig. 2.3C). One potential hypothesis is that baseline VOR gain might require a longer time to change, while VOR adaptation is affected immediately. To test this, I measured the baseline VOR gain from a subset of the CRISPRa treated mice a month after the first recording session, as well as from the Cre injected *Scn2a*$^{+/fl}$ mice two months after their first recording session. None of these mice showed changes in baseline VOR gain when comparing the two timepoints (Fig. 3.2). This suggests even more strongly that baseline VOR gain might be developmental dependent and has been set during a critical period.

Immunohistochemistry staining for mCherry showed incomplete but uniform infection of the construct in the cerebellum (Fig. 3.1B). It is worth noting that unlike the CRISPRa with *Scn2a* sgRNA construct, this mCherry construct is not cell type specific,

which explains why it is also expressed in other neurons other than granule cells such as Purkinje cells. Although this approach does not address whether the cerebellum is sufficient for VOR adaptation, the ability to rescue targeted gene expression through a systemic delivery method might be more clinically relevant and therapeutically beneficial.

To assess whether loss of *SCN2A* affects VOR behavior in human, we recruited 5 children with *SCN2A* LoF variants and 11 neurotypical children as control subjects, all of whom were aged 3-10 years old. Children were instructed to sit in the rotating chair by themselves or on the lap of one of their parents or caregivers in the chair, whichever they felt the most comfortable with. Their eye movement was then calibrated in a dimmed environment where they were instructed to hold their head still while keep their gaze on a stuffed animal that was being moved between two points that were 10 degrees apart with the origin from the location of the rotating chair. After calibration, we performed VOR recordings in both dimmed and completely dark environment. We only extracted eye tracking data from the dark session for analysis, while the short, dimmed session served as a habituation period for the children.

Neurotypical children exhibited a similar baseline VOR gain value comparing with the WT mice (Fig. 3.4B, D, E). However, children with *SCN2A* LoF children presented with elevated gain near unity (Fig. B, D, E). As an evolutionarily conserved oculo-motor reflex, of which the existence has been found spanning across Mammalia, it is expected that the neural circuitry underlying this reflex should be similar. Indeed, we were able to observe that the same genetic loss can lead to almost identical behavioral phenotypes in human and mouse.

In conclusion, I was able to utilize the existing CRISPRa construct combined with systemic ROA technique to elevate Scn2a expression in mice. Meanwhile, I showed that this is sufficient to rescue VOR adaptation ability in these mice by returning their Purkinje cell activity to similar to WT level during and after gain-down induction. In addition, we observed a similarly elevated VOR gain in children with *SCN2A* LoF variants compared to the *Scn2a*$^{+/-}$ mice. Last but not least, we are very grateful for all children, parents, and caregivers at the FamilieSCN2A Foundation for participating in this study.

Conclusions

This four-year long thesis project touched upon many aspects of modern neuroscience research to address the question of how *Scn2a* haploinsufficiency alters cerebellar physiology and relevant behaviors. Using patch clamp whole-cell recording in acute *ex vivo* cerebellar tissue, I was able to dissect the effects of *Scn2a* loss on the principal pathway in cerebellar cortex. Insufficient $Na_V1.2$ expression in granule cells reduced their intrinsic excitability, which might raise the threshold of sensory input filtering via mossy fibers. Impaired ability to sustain long, high-frequency FV train along the parallel fibers could alter the AP fidelity at the axonal terminals. Indeed, when attempted to induce LTP at the granule cell to Purkinje cell synapse in *Scn2a*$^{+/-}$ condition by eliciting AP bursts in parallel fibers, there was no potentiation observed. Moreover, impaired short-term facilitation measured in the total charge transfer of the EPSCs suggests that any baseline synaptic transmission might also be affected. This synaptic impairment might drive any behavioral phenotype that is dependent on cerebellar plasticity. Assessing a cerebellar-modulated oculo-motor reflex, VOR, on mice with *Scn2a* haploinsufficiency not only revealed an abnormally high VOR gain, but also uncovered the deficit in VOR gain-down adaptation. *In vivo* extracellular recording of Purkinje cell activity in the floccular complex during VOR confirmed a direct correlation between the ability, or inability, to adapt to VOR learning and Purkinje cell simple spike frequency. Restricting *Scn2a* heterozygosity mostly in the cerebellum produced the same behavioral and physiological phenotypes. Finally, utilizing a potential gene therapy candidate, CRISPRa, rescued not only the *Scn2a* expression level in mice, but also their ability in VOR gain-down adaptation. This work illustrated that there are aspects of behavioral deficits caused by

Scn2a haploinsufficiency can be reversed by restoring the gene expression later in adulthood in mice. Our preliminary findings revealed that children who carry *SCN2A* LoF variants also exhibit saturated baseline VOR gain almost identical to what was observed in mice. This similarity between mouse and human gives us the optimism that engineering successful therapeutic strategies for not only *SCN2A*-related disorders, but also ASD and neurodevelopment disorders in general might not be too far in the horizon.

Figures

Chapter 1 Figures

Figure 1.1

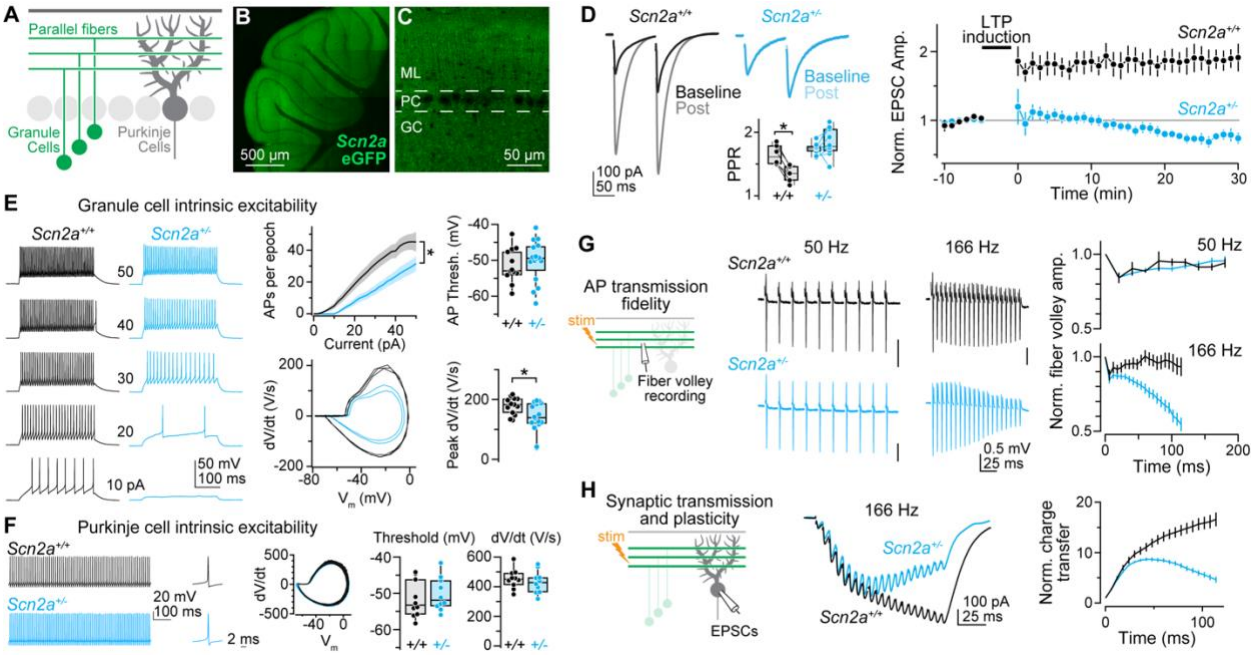

Figure 1.1: Impaired cerebellar granule cell excitability and plasticity in *Scn2a*$^{+/-}$ conditions.

A: Schematic of excitatory circuit between granule cells and Purkinje cells. Subsequent panels highlight different circuit components under investigation.

B: Coronal section of the mouse cerebellum in animal with eGFP knocked into the *Scn2a* locus. Note GFP expression in granule cell layer and molecular layer and lack of expressing in Purkinje cell layer.

C: Coronal section through cerebellar vermis, perpendicular to major axis of Purkinje cell dendrites. Note periodicity of staining in molecular layer, consistent with lack of expression in Purkinje cell dendrites.

D: Left: Two EPSCs (10 Hz) before and after 166 Hz burst LTP induction in *Scn2a*$^{+/+}$ (black, n = 6 cells from 6 mice) and *Scn2a*$^{+/-}$ (cyan, n = 10 cells from 4 mice). Inset, paired pulse ratio before and after LTP induction. *: $p < 0.01$, Wilcoxon signed-rank test. Right, first EPSC amplitude, normalized to pre-induction average. Data are binned each minute. Circles and bars are mean ± SEM.

E: Left: APs generated by current injection (10-50 pA, 300 ms) in *Scn2a*$^{+/+}$ (black) and *Scn2a*$^{+/-}$ (cyan). Middle: APs (spikes) per 300 ms stimulation epoch for each current amplitude (top; lines and shadow are mean ± SEM of population, *: $p < 0.05$ of slope between 10-40 pA), and near-rheobase APs plotted as dV/dt vs voltage (phase-plane plot) from *Scn2a*$^{+/+}$ and *Scn2a*$^{+/-}$. Right: AP threshold (top) and peak dV/dt (bottom) in *Scn2a*$^{+/+}$ (13 cells from 3 mice) and *Scn2a*$^{+/-}$ (16 cells from 3 mice). *: $p < 0.05$, Mann Whitney test. Circles are single cells, boxes are medians and quartiles with 90% tails.

F: Left to right: spontaneous Purkinje cell AP train in *Scn2a*$^{+/+}$ and *Scn2a*$^{+/-}$, single AP, phase-plane plot of all APs in train, and summary AP threshold and peak dV/dt in *Scn2a*$^{+/+}$ and *Scn2a*$^{+/-}$.

G: Left, Parallel fiber volleys evoked in trains of 10 APs at 50 Hz or 20 APs at 166 Hz. Right, Fiber volley amplitude, normalized per volley to first event in train, then averaged across recordings. Lines and bars are mean ± SEM. 50 Hz (top) in *Scn2a*$^{+/+}$ (black, n = 5 from 2 mice) and *Scn2a*$^{+/-}$ (cyan, n = 7 from 4 mice). 166 Hz (bottom) in *Scn2a*$^{+/+}$ (black, n = 9 from 3 mice) and *Scn2a*$^{+/-}$ (cyan, n = 9 from 4 mice).

H: Left, parallel fiber evoked EPSCs in Purkinje cells from train of 20 stimuli at 166 Hz. Right, charge transfer, normalized to transfer from EPSC1 in *Scn2a*$^{+/+}$ (black, n = 10 cells from 2 mice) and *Scn2a*$^{+/-}$ (cyan, n = 9 cells from 2 mice) conditions.

Chapter 2 Figures

Figure 2.1

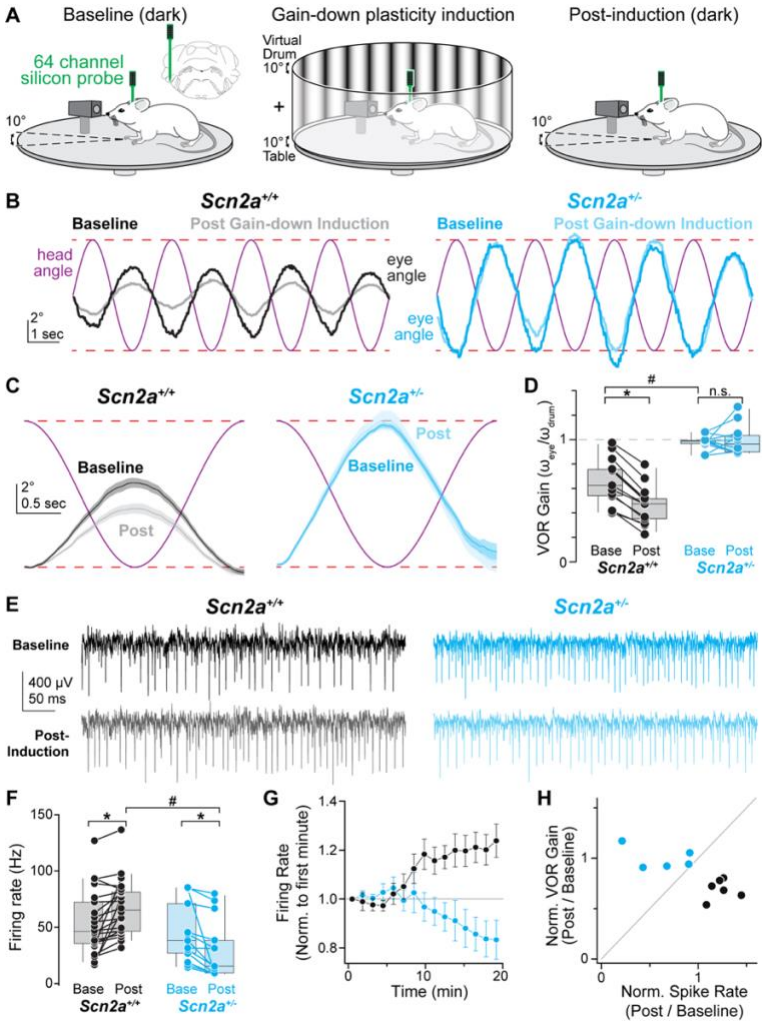

Figure 2.1: Impaired VOR gain-down behavioral plasticity in *Scn2a*$^{+/-}$ mice.

A: Experimental design for VOR gain-down induction and simultaneous *in vivo* silicon probe recording in the cerebellar floccular complex. Inset, recording location in left hemisphere. Left: baseline VOR recording in the dark. Middle: VOR gain-down induction with virtual drum as visual stimulus. During gain-down induction, visual stimulus was moved in phase with table. Right: post-induction VOR recording in the dark.

B: Head and eye angles in *Scn2a*$^{+/+}$ (black) and *Scn2a*$^{+/-}$ (cyan) during baseline (dark colors) and post-induction (light colors) with table rotation (purple). Dashed red lines indicate ±5° range.

C: Head angle (purple) and contraversive eye angle before (darker shade) and after (lighter shade) gain-down induction. Data presented as in Fig. 3.4D.

D: VOR gain before and after gain-down induction. Data color coded as in B. Bars connect data from individual mice. * $p < 0.001$, Wilcoxon signed rank test, # $p < 0.0001$, Mann Whitney test.

E: Putative Purkinje cell unit recordings before and after gain-down induction. Traces are aligned from table rotation onset.

F: Average Purkinje cell simple spike firing frequency during sinusoidal head rotation, before and after gain-down induction, displayed as in D. *Scn2a*$^{+/+}$ (black, closed circles, n = 22 units, 6 mice), *Scn2a*$^{+/-}$ mice (cyan, n = 13 units, 5 mice). * $p < 0.05$, all conditions, Mixed-effects modeling, # $p < 0.001$, Wilcoxon signed rank test.

G: Normalized Purkinje cell simple spike firing frequency during induction protocol, normalized to firing rate in first minute per unit. Circles and bars are mean ± SEM, binned per minute.

H: Normalized change in VOR gain vs. normalized change in simple spike rate (normalized per unit and averaged across units per animal). Circles are color-coded as in panel D and represent individual animals.

Figure 2.2

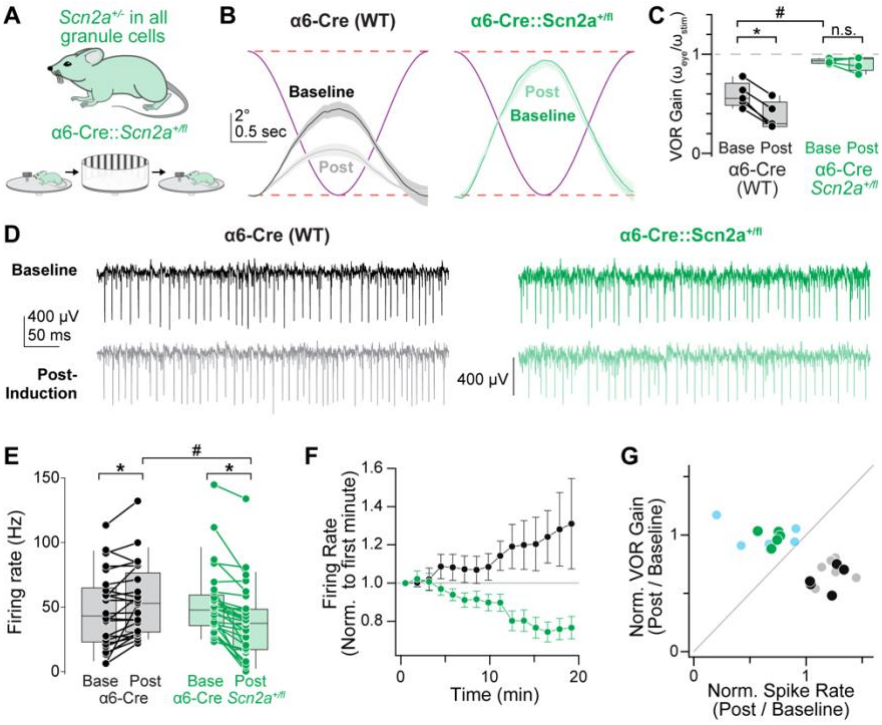

Figure 2.2: *Scn2a* heterozygosity in granule cells alone impairs VOR gain-down plasticity.

A: Experimental design for VOR gain-down induction as in Fig. 2.1, but for *Scn2a*$^{+/fl}$ mice crossed to the alpha6-Cre driver line (α6-Cre), which restricts Cre expression largely to cerebellar granule cells.

B: Head angle (purple) and contraversive eye angle before (darker shade) and after (lighter shade) gain-down induction for α6-Cre not crossed to *Scn2a*$^{+/fl}$ animals (black, WT-equivalent), or α6-Cre::*Scn2a*$^{+/fl}$ mice (green).

C: VOR gain before and after gain-down induction. Data color coded as in B. Bars connect data from individual mice. *: $p < 0.001$, Wilcoxon signed rank test, # $p < 0.0001$, Mann Whitney test.

D: Putative Purkinje cell unit recordings before and after gain-down induction. Traces aligned to table rotation onset.

E: Average Purkinje cell simple spike firing frequency during sinusoidal head rotation, before and after gain-down induction, displayed as in C. α6-Cre WT (gray, open circles, n = 24 units, 5 mice) and α6-Cre::*Scn2a*$^{+/fl}$ mice (green, n = 28 units, 5 mice). *: $p < 0.005$, all conditions, Mixed-effects modeling, #: $p = 0.01$, Mann Whitney test.

F: Average Purkinje cell simple spike firing frequency during induction protocol, normalized to firing rate in first minute per cell. Circles and bars are mean ± SEM, binned per minute.

G: Normalized change in VOR gain vs. normalized change in simple spike rate (normalized per unit and averaged across units per animal). Circles are color-coded as in C and represent individual animals. Data from *Scn2a*$^{+/+}$ (gray) and *Scn2a*$^{+/-}$ (light cyan) are in background for comparison.

Figure 2.3

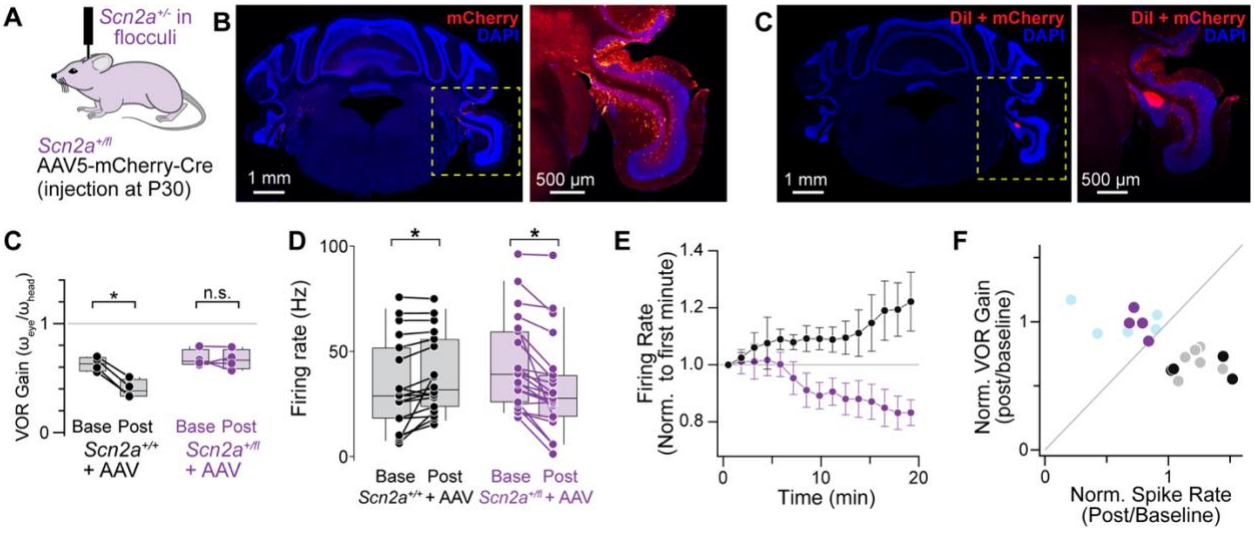

Figure 2.3: *Scn2a* heterozygosity induced only in the floccular complex impairs VOR behavioral plasticity.

A: AAV5-mCherry-Cre was injected bilaterally into the floccular complex in *Scn2a*$^{+/fl}$ mice at P30.

B: Coronal section through floccular complex detailing mCherry expression. Yellow dashed box is expanded on right, using the "red-hot" lookup table (ImageJ) for mCherry fluorescence.

C: Coronal section detailing identification of silicon probe with DiI in animal previously injected with AAV5-mCherry-Cre.

D: VOR gain before and after gain-down induction in *Scn2a*$^{+/+}$ mice with Cre (black, N = 4 mice) and *Scn2a*$^{+/fl}$ with Cre (purple, N = 4 mice). *: p = 0.029, Wilcoxon signed rank test.

E: Average Purkinje cell simple spike firing frequency during sinusoidal head rotation, before and after gain-down induction in *Scn2a*$^{+/+}$ with Cre (red, n = 18 units from 4 mice) and *Scn2a*$^{+/fl}$ with Cre (purple, n = 21 units from 4 mice). *: $p < 0.05$, Mixed-effects modeling.

F: Normalized Purkinje cell simple spike firing frequency during gain-down induction. Data are binned every minute. Circles and bars are mean ± SEM.

G: Normalized VOR gain vs normalized simple spike firing frequency following gain-down induction for each mouse. *Scn2a*$^{+/+}$ (gray) and *Scn2a*$^{+/-}$ (light blue) data are displayed for comparison.

Figure 2.4

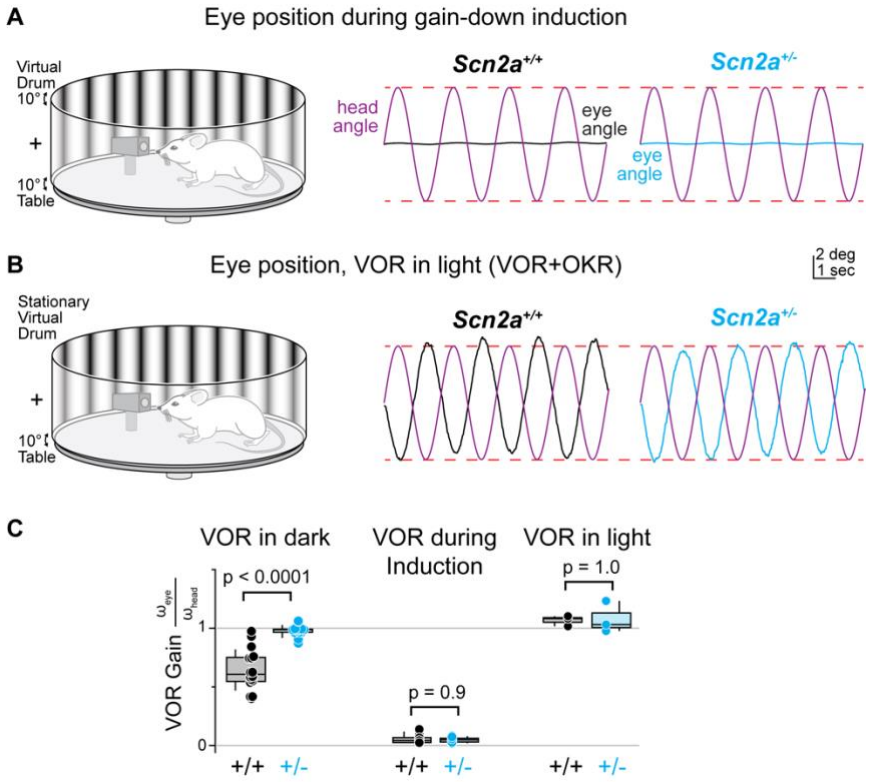

Figure 2.4: Eye movement during gain-down induction and VOR in light.

A: Left: schematic of experimental setup for VOR gain-down induction. Right: example of eye position during VOR gain-down induction in WT and *Scn2a*$^{+/-}$ mice.

B: Left: schematic of experimental setup for VOR in light, where the mouse is rotated while the visual stimulus remains fixed. Right, example eye position in WT and *Scn2a*$^{+/-}$ mice.

C: Data summarizing gain during VOR in the dark (left), during gain-down induction (middle), and VOR in light (right). Circles are animals, boxes are medians and quartiles with 90% tails. P-values are for Mann-Whitney comparisons.

Figure 2.5

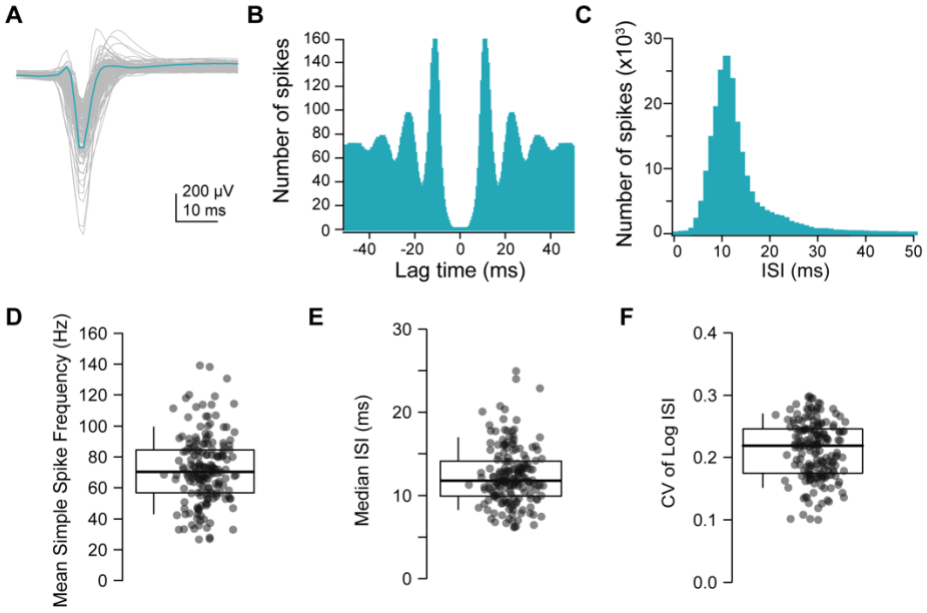

Figure 2.5: Properties of putative Purkinje cell simple spike units.

A: Overlayed median simple spikes waveform from each putative Purkinje cell unit in all mice (144 units from 39 animals).

B: Autocorrelogram of the example Purkinje cell unit in A during the entire recording session.

C: Inter-spike interval distribution of the example Purkinje cell unit in A.

D: Distribution of mean simple spike firing frequency from all included Purkinje cell units.

E: Distribution of median inter-spike interval (ISI) from all included Purkinje cell units.

F: Distribution of the coefficient of variation of the natural log of the ISIs from all included Purkinje cell units.

In each panel, circles are units. Boxes are median and quartiles, with 90% tails.

Chapter 3 Figures

Figure 3.1

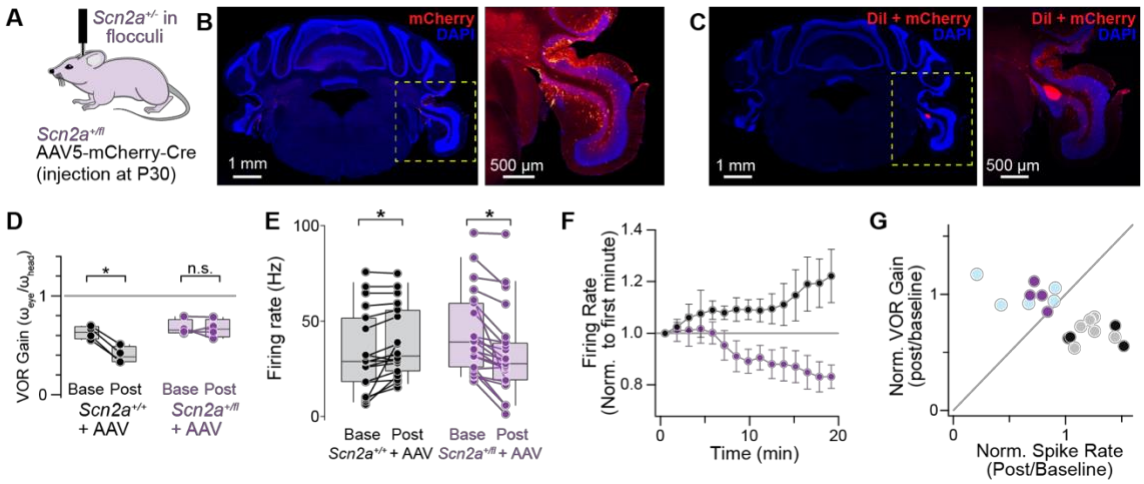

Figure 3.1: Rescue of VOR gain-down behavioral plasticity with CRISPR activation.

A: Two AAV-PHP vectors are injected together for systemic infection via the retro-orbital sinus. AAV1 contains a guide RNA and mCherry. AAV2 contains dCas9 and the transcriptional regulator VP64.

B: Cerebellar coronal section from injected animal. Note broad, but incomplete, infection across cerebellum, as signaled by mCherry fluorescence. A region of cerebellum containing the left floccular complex was dissected immediately after harvesting brain for quantitative PCR and is missing from section.

C. Quantitative PCR result showing *Scn2a* mRNA detection in mouse cerebellum of "empty vector" controls, which contain all viral elements except the guide RNA. In 5/6 animals, marked upregulation was noted (closed circles). In 1 animal, no upregulation was noted (open circle).

D: VOR gain before and after gain-down induction in *Scn2a*$^{+/-}$ mice with *Scn2a* CRISPRa (red, 6 mice) and empty vector (blue, 4 mice), depicted as in Fig 2.1D. *: $p < 0.05$ Wilcoxon-signed rank test; all data included.

E: Average Purkinje cell simple spike firing frequency during sinusoidal head rotation, before and after gain-down induction in *Scn2a*$^{+/-}$ mice with CRISPRa (red, n = 28 units from 6 mice) and empty vector (blue, n = 25 units from 4 mice). Circles are color-coded as in D and represent individual units. *: $p < 0.005$, Mixed-effects modeling.

F: Normalized Purkinje cell simple spike firing frequency during gain-down induction for all CRISPRa (6 mice) and empty vector (4 mice) injected animals. Circles and bars are mean ± SEM, binned per minute.

G: Normalized change in VOR gain vs. normalized change in simple spike rate (normalized per unit and averaged across units per animal). Circles are color-coded as in D and represent individual units. Data from *Scn2a*$^{+/+}$ (gray) and *Scn2a*$^{+/-}$ (light cyan) are in background for comparison. Note overlap of CRISPRa population with *Scn2a*$^{+/-}$ population (except open circle) and empty vector with *Scn2a*$^{+/-}$ population.

Figure 3.2

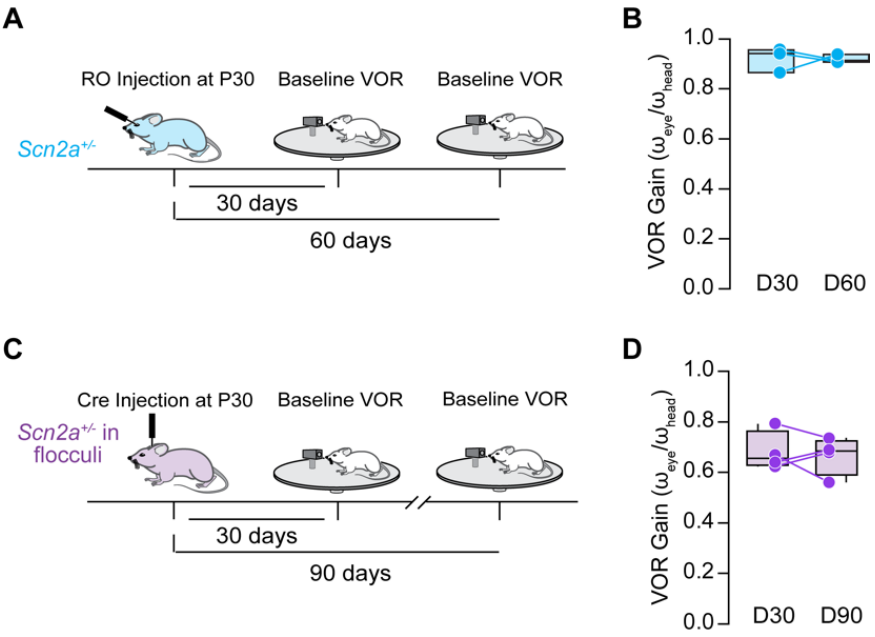

Figure 3.2: Baseline VOR gain remains unchanged after manipulations of *Scn2a* expression from P30.
A: Timeline of CRISPRa RO injection (at P30) and VOR recordings (30 days and 60 days after injection).
B: Data summarizing baseline VOR gain at post-injection day 30 and day 60 in *Scn2a*$^{+/-}$ mice with *Scn2a* CRISPRa.
C: Timeline of Cre injection (at P30) and VOR recordings (30 days and 90 days after injection).
D: Data summarizing baseline VOR gain at post-injection day 30 and day 90 in *Scn2a*$^{+/fl}$ mice with Cre.

Figure 3.3

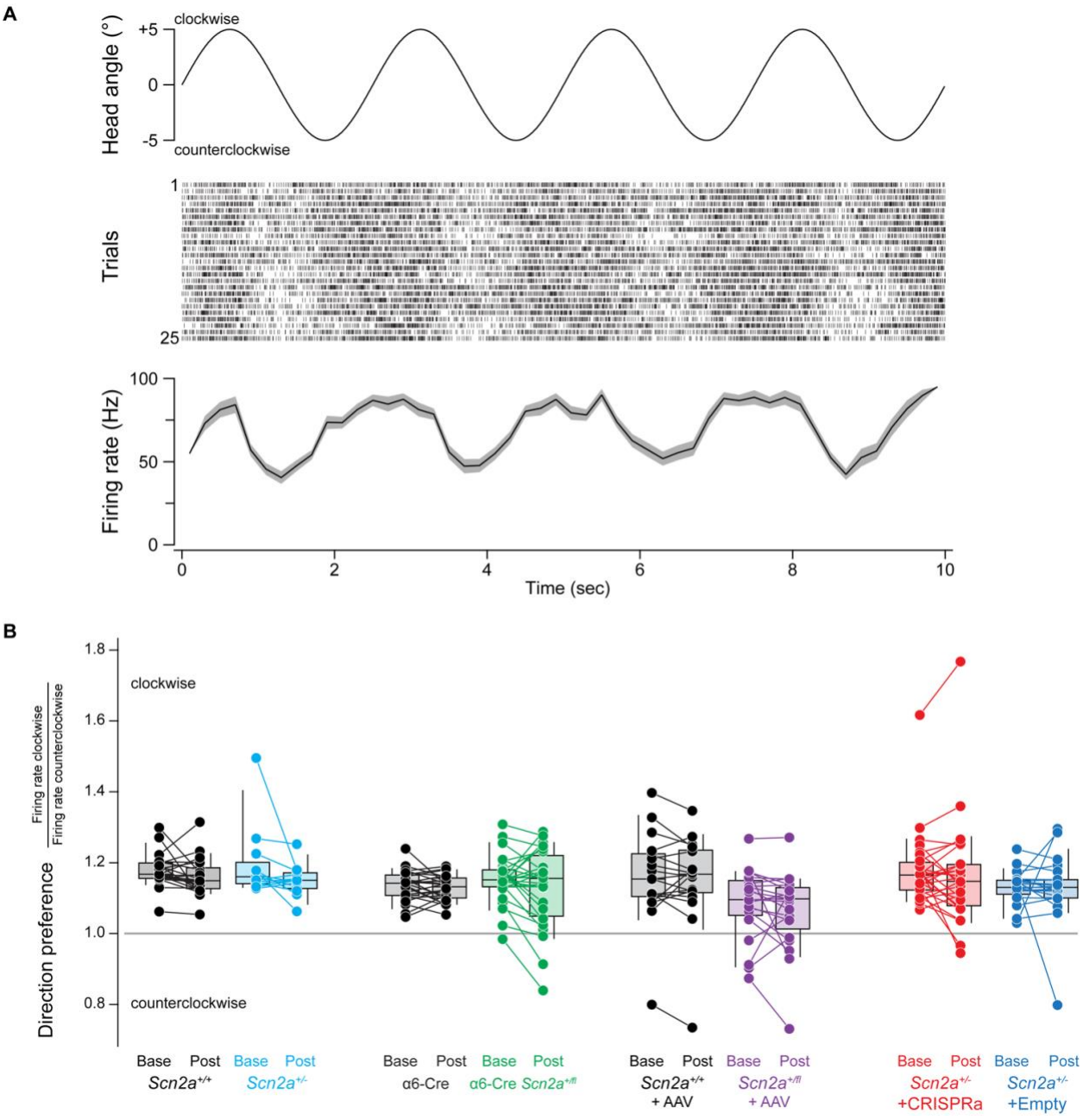

Figure 3.3: Putative Purkinje simple spiking units display directional bias to head rotation.

A: Example Purkinje cell unit activity during table rotation (VOR baseline, WT animal). Top is head angle. Middle is simple spike raster across all 25 trials. Bottom is mean ± SEM firing rate, binned every 200 ms.

B: Summary direction preference (total spikes during clockwise movement / total spikes during counterclockwise movement) for each unit across all conditions. Circles are single units; lines connect individual units. Box plots are medians and quartiles with 90% tails. Note that the majority of units prefer clockwise movement.

Figure 3.4

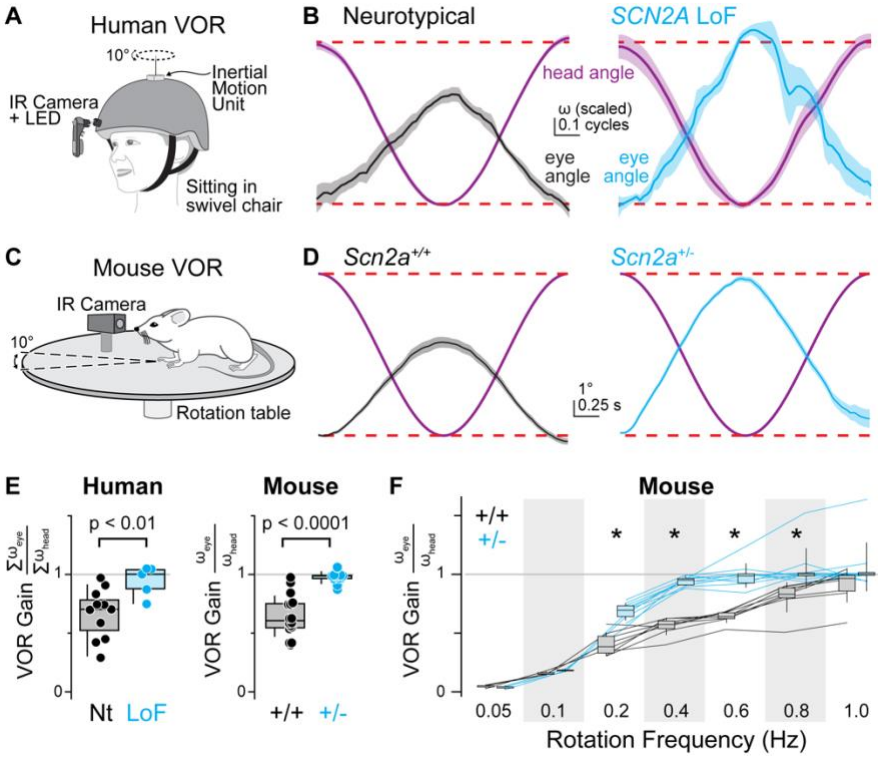

Figure 3.4: VOR gain is elevated in *Scn2a* haploinsufficiency conditions.

A: Schematic of purpose-built eye tracking apparatus for VOR assessment in children. Head movements are measured from a device located at the center of the head while the right eye is imaged under infrared illumination (940 nm LED). Participants are seated in a swivel chair and oscillated ±5° at ~0.4 Hz to assess VOR gain.

B: Head angle (purple) and contraversive eye angle for neurotypical (Nt, black) and *SCN2A* LoF conditions (cyan). Lines represent the average of a single cycle from all participants; shaded area is SEM. Dashed red lines indicate ±5° range.

C: VOR was assessed in mice head-fixed at the center of a rotating table, imaged under IR illumination.

D: VOR at 0.4 Hz rotation frequency, displayed as in panel B, for *Scn2a*$^{+/+}$ (left, black) and *Scn2a*$^{+/-}$ mice (right, cyan).

E: Baseline VOR gain in human and mouse. Circles are individuals; box plots are medians, quartiles and 90% tails. n: 11 Nt, 5 LoF humans; 13 +/+, 12 +/- mice. Mann Whitney test p-values shown.

F: VOR gain across rotation frequencies in mouse. Lines connect repeated tests in single mice. Asterisks: $p < 0.0001$, Friedman test on overall distribution; Mann Whitney test on individual frequencies, Holm Šídák correction.

Figure 3.5

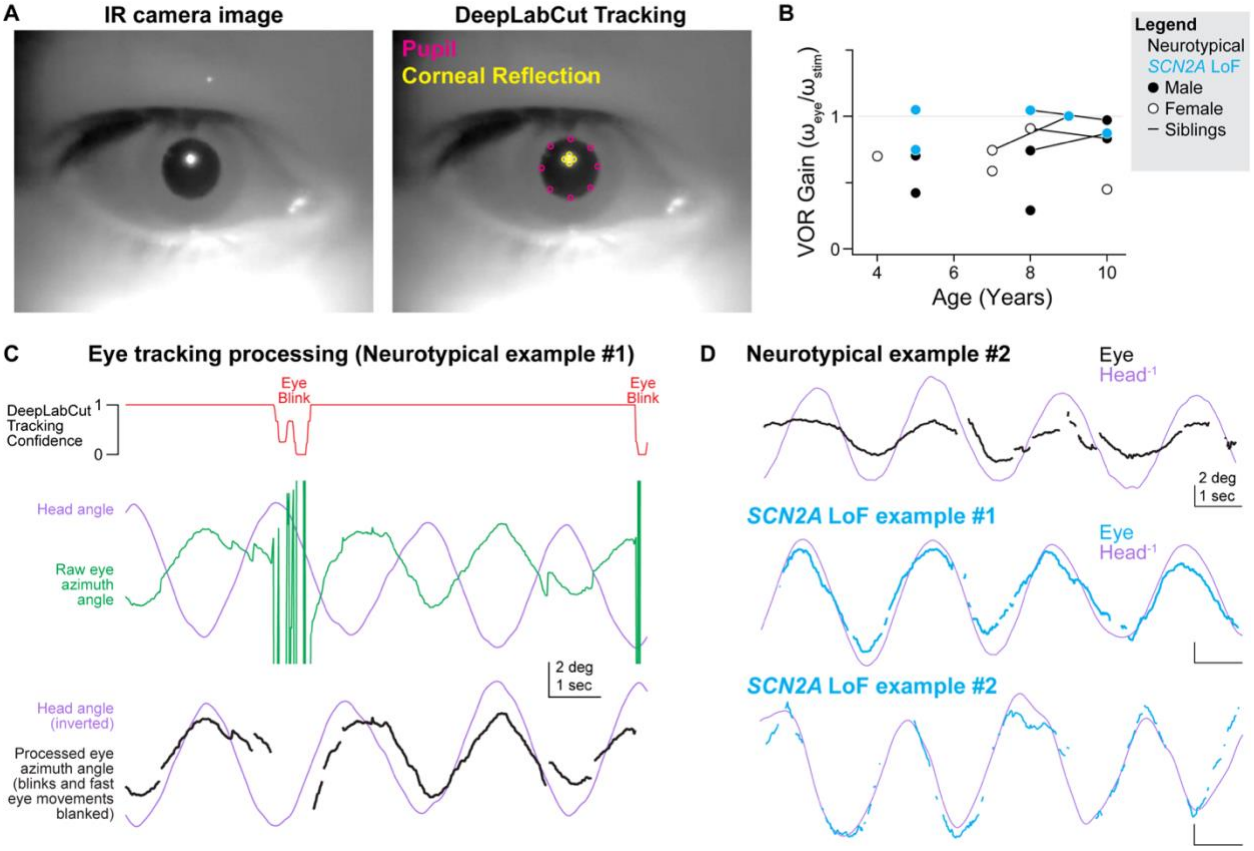

Figure 3.5: Human VOR analysis.

A: Example infrared image of right eye (left) and overlaid DeepLabCut tracking of pupil boundaries and corneal reflection (right). Landmarks were tracked at 8 and 4 locations near areas of maximal contrast to minimize tracking errors. Azimuth position was calculated by averaging across all points.

B: VOR gain per subject across age, coded by sex and *SCN2A* phenotype. Siblings are connected by lines.

C: Analysis pipeline for VOR quantification. Top: Red trace is average DeepLabCut confidence metric of marker position. Middle: purple trace is head angle determined from inertial motion unit. Green trace is raw DeepLabCut eye angle. Bottom: Black trace shows post-processing of eye position after periods of low DeepLabCut confidence and periods where eyes move >20°/s are blanked. Note that the head never moved faster than 12.5°/s during 0.4 Hz rotations.

D: Other examples of post-processed eye and head angle in neurotypical and *SCN2A* LoF children.

Methods

Human vestibulo-ocular reflex:

Experiments were performed on children of either sex, aged 3-10 years. All procedures were in accordance with UCSF IRB guidelines and parental consent was obtained for all participants. Inclusion criteria for *SCN2A* loss-of-function (LoF) children included those with a genetic diagnosis of *SCN2A* dysfunction and a diagnosis of autism spectrum disorder and neurodevelopmental delay. Furthermore, children were limited to those without seizure or any seizure-related medication within the last 6 months. Neurotypical (Nt) children were limited to those that did not present with neurodevelopmental delay, autism spectrum disorder, or seizure.

For VOR experiments, children were seated in a standard office executive chair with the center of their head situated near the azimuth swivel. Children were either seated alone or in a caregiver's lap for both Nt and LoF cohorts, with no discernable differences in data quality due to caregiver presence. Children were then fitted with a helmet (67i skateboard helmet, child's small or medium depending on participant, Amazon) that was kitted with an inertial movement unit centered at the top of the helmet and an infrared camera (Raspberry Pi NoIR) and 940 nm LED (Luxeon star) with a 10° diffuser lens focused on the right eye. The camera was aligned to ensure that a corneal reflection from the LED could be visualized. Eye movement was first calibrated in light conditions by having children attend to a visual stimulus (a chirping yellow sparrow stuffed animal or a pen light clicked on and off as conditions permitted) moved back and forth from a position either directly ahead or 10 degrees offset. Calibration was repeated >4x for each child and eye position calibration tracking was averaged over all trials.

Following calibration, the chair was rocked back and forth ~±5° at ~0.4 Hz in the dark by an experimenter wearing night-vision optics, with oscillations paced by a metronome. Videography and IMU data were acquired at 60 and 300 Hz, respectively. IMU data were downsampled to 60 Hz for subsequent analysis.

Data acquisition could not be performed blind to LoF/Nt condition given the phenotypes being analyzed. All data was therefore coded and blinded for subsequent analysis. Post-hoc processing of eye position was performed using DeepLabCut 2.0 Toolbox (deeplabcut.org) [87]. DeepLabCut was trained by an experimenter to detect 8 points at regions of maximal contrast at the edge of the pupil (every 45 degrees) and 4 points at the edge of the corneal reflection (every 90 degrees). Horizontal eye angle was calculated as the average horizontal pupil value (all 8 points) relative to the average horizontal corneal reflection value (all 4 points). Data acquired during VOR tests were then normalized to calibration sets to obtain the exact eye movement angle.

All children naturally made saccades and blinked during data acquisition. These events were removed from subsequent analysis by eliminating all data when eye movement speed exceeded 20 deg/sec and where the DeepLabCut position “confidence” value, averaged over all 12 imaged points, was <0.99 (range: 0 to 1.0). Eye angle and head angular velocity (IMU) data were used to calculate instantaneous velocity, smoothed with a 2 data-point-wide Gaussian filter. VOR gain was then calculated as the ratio of the integral of absolute values of instantaneous eye velocity and corresponding values of head velocity over the entire recording epoch (Fig. 3,5).

Animals:

All experimental procedures were performed in accordance with UCSF IACUC guidelines. All experiments were performed on mice housed under standard conditions with *ad libitum* access to food and water, with colonies maintained in-house. Wild-type C57B6J were from JAX (000664); Alpha6-Cre mice were initially described in Bahn et al., 1997 [88]; *Scn2a*$^{+/-}$ mice were initially described in Plannels-Cases, 2000 [89]; conditional knockout *Scn2a* allele mice were initially described in Spratt et al., 2019 [9]; conditional knockin *Scn2a* mice with GFP in-frame were described in Tamura et al., 2022 [84].

Surgical procedures:

Head Plate Implantation for Head-fixed Recordings

Mice were implanted with a head bar composed of three threaded screw inserts arranged in a triangle (McMaster-Carr, 92395A109) at least 14 days before recording. Mice were anesthetized with 2% isoflurane. The scalp was shaved and disinfected with povidone iodine. The scalp was resected, and the skull was scored with a sterilized bone scraper. The edge of the skin was glued to the skull and the metal threaded screw inserts were sterilized and mounted using Metabond and dental cement (Ortho-Jet powder; Lang Dental) mixed with black paint (iron oxide). The inserts were mounted via a stereotax with the triangular center aligned to bregma. Following the implantation, black dental cement was used to build a recording well surrounding the skull above the targeted floccular complex region at (from the bregma, in mm): anterior-posterior, -5.40, mediolateral, -2.75. The surface of the skull above the left hemisphere of the cerebellum was not covered with dental cement but was coated with a thin layer of transparent cyanoacrylate glue. Mice

were injected intraperitoneally with 0.1 mg/kg buprenorphine before and after surgery and were checked daily for 3 days after the head-bar surgery.

Craniotomy for Electrophysiological Recordings

Following the last day of habituation to head fixation, each mouse was anesthetized with 2% isoflurane and the skull above the recording site was drilled off. The dura was not removed, and the craniotomy was kept moist with phosphate buffered saline (PBS). Following craniotomy, the window was sealed with biocompatible silicone sealant until the recording session (Kwik-Cast, World Precision Instruments).

Stereotaxic transcranial viral injection

Mice with one conditional knockout *Scn2a* (*Scn2a*$^{+/fl}$) allele at P30 were anesthetized under isoflurane at 2.0% and mounted onto the stereotaxic machine (Kopf 1900). 500 nL of AAV-EF1a-mCherry-IRES-Cre-WPRE (UNC Vector Core) was injected into the floccular complexes on both sides at (from the bregma, in mm): anterior-posterior, -5.40; mediolateral, ±2.75; dorsoventral: −4.00 at 100 nL per minute.

Viral injection via retro-orbital sinus

AAV-PhP.eb-CMV-sadCas9-VP64 with either AAV-PhP.eb-U6-sasgRNA-CMV-mCherry (CRISPRa) or an empty vector containing AAV-PhP.eb-U6-CMV-mCherry suspended in 5% Sorbitol (Sigma-Aldrich, Inc.) at a total volume of 150 µL and packaged in a 28-gauge needle with 0.5 mL insulin syringe (U-100; Becton, Dickinson and Company). Mice aged P30 were anesthetized under inhalant isoflurane and were kept

warm on a heating pad. Ophthalmic ointment (Puralube Vet Ointment; Dechra) was applied to both eyes of the anesthetized mouse. The mouse was then laid on its left side and the needle was subsequently inserted into the medial canthus underneath the left eyeball until it reached the base. The mixture of viral constructs was then introduced into the retro-orbital sinus. After a 10-second pause, the needle was slowly withdrawn and additional ocular ointment was applied. The mice were monitored for signs of bleeding (none noted) and provided analgesic and monitored for pain for 3 days post-injection [86].

Behavior:

Habituation and eye calibration

Behavioral experiments were performed during the light cycle and the experimenter was blind for genotype during experiment and analysis. After allowing for at least 1 week of recovery after surgery, each mouse was habituated to the experimental setup by head-fixing it in a purpose-built restraining tube with a head holder that was positioned at the center of the turntable for 1-2 hours each day for 4 consecutive days [90]. Each mouse was habituated for 1 hour in the darkness on the first day, then with a 20-minute increment on each subsequent day for the following three days.

On the third habituation day, the right eye of each mouse was calibrated using a standard method, as reported previously[90]. Briefly, to calibrate eye movement, we used a corneal reflection generated by an infrared LED as a reference position for the eye. A static virtual drum was presented during calibration. After identifying the pupil and the center of the eye, the camera and the reference LED were rotated by 10 degrees in both directions to acquire the distance between the pupil reference and the pupil center. The

pupil size was varied by changing the luminance of the virtual drum to obtain increase the dynamic range of pupil size values.

Vestibulo-ocular reflex recordings

Mice were given 3% topical pilocarpine HCl in both eyes 15 minutes prior to the beginning of each VOR recording session to temporarily restrict their pupil size in the dark. Compensatory eye movements were recorded using video-oculography. The velocity of head movements was controlled by the servo-controlled platform that enabled the rotation of the animal along the horizontal plane. The platform was attached to a gearbox 15:1 (VTR010-015-RM-71 VTR, Thomson) that increased the torque of a servo motor (AKM53L-ANC2C-00 KEC0432 AC Servomotor 1.83 kW, Kolmorgen). The motor was tuned using a servo drive (AKDB013206-NBAN-0000 servo drive, Kolmorgen) and controlled in velocity mode using analog waveforms computed in LabView 2020 (NI). The head of each mouse was positioned with a 20 degrees angle along the sagittal plane of the head (nose pointing 20 degrees down), such that the plane of the horizontal vestibular canal was approximately parallel to the plane of the rotating platform. VOR was evoked by rotating the platform in the dark with 5° amplitude in each direction and a temporal frequency of 0.4 Hz unless otherwise stated. Gain-down VOR induction protocol was performed by presenting a coherent virtual drum with a spatial frequency of 0.8 Hz and a temporal frequency of 0.4 Hz with the platform rotation that oscillates in the same direction to evoke near complete VOR cancellation (see Fig. 2.4A).

***In vivo* Extracellular recordings:**

All recordings in this study were performed in the left floccular complex (contralateral to the imaged eye). Extracellular recordings were performed using a 2-shank silicon probe that is 8 mm in length and contains 32 channels on each shank with 25 µm inter-channel distance and 250 µm inter-shank distance (ASSY-77 H2, Cambridge Neurotech). The recording electrode was controlled with a micromanipulator (MP-285; Sutter Instrument) and stained with DiI lipophilic dye (Thermo Fisher) for post-hoc identification of the electrode location (see Fig. 2.3C). The signals were acquired at 30 kHz using an INTAN system (RHD2000 USB Interface Board, INTAN Technologies). Recordings in the floccular complex were performed at (from bregma, in mm): anterior-posterior, -5.40; mediolateral, -2.75; dorsoventral: −4.00.

On the day of recording, each mouse was head-fixed on the VOR experiment setup. The silicon sealant was then removed, and the craniotomy was kept moist with artificial cerebrospinal fluid contained (in mM): 140 NaCl, 5 KCl, 10 D-glucose, 10 HEPES, 2 CaCl2, 2 MgSO4 with a pH of 7.4. The recording electrode was lowered into the left floccular complex via the craniotomy at a speed of ~250 µm per minute. Experiments began at least 50 minutes after reaching the final electrode depth to allow for electrode stabilization.

Histology:

For anatomical analysis, mice were perfused transcardially with phosphate buffered saline (PBS, Sigma-Aldrich) and then with 4% paraformaldehyde (PFA, VWR International, Inc.) in PBS. Brains were extracted from the skulls, post-fixed in 4% PFA

overnight at 4°C, switched to 15% sucrose in PBS for 4 hours, and then stored in 30% sucrose in PBS until sectioned. Sequential coronal sections of the cerebellum (30 μm) were collected with a Microm HM 525 Cryostat and were stored in 0.05% sodium azide (Sigma-Aldrich) in PBS. For *in vivo* recording electrode location identification, sections were rinsed in 1X PBS 3 times for 15 minutes and then were then coverslipped with ProLong Gold with DAPI (Life Technologies). For immunohistochemistry mCherry staining, sections were rinsed in 1X PBS 3 times for 15 minutes and then incubated overnight at 4°C with 10% normal goat serum (Fisher Scientific) with 0.2% Triton X-100 (Sigma-Aldrich) and Anti-RFP (Rabbit) primary antibodies (1:1000) (Rockland Immunochemicals). The next morning, sections were kept at room temperature for 1 hour before being rinsed with 1X PBS 3 times for 15 minutes. The sections were then incubated with Alexa Fluor 568 goat anti-rabbit (1:500) (Invitrogen) for 2 hours at room temperature. Sections were then coverslipped with ProLong Gold with DAPI (Life Technologies). Fluorescence images were acquired using an Olympus FV3000 confocal microscope under 4x or 20x objectives.

Data Analysis:

Monitoring eye movements by video-oculography

The movement of the right eye was monitored using a high-speed infrared (IR) camera (IPX-VGA210LMCN; Imperx, Inc.) by capturing the reflection of the eye on an IR mirror (Edmund Optics #64–471) that is transparent to visible light under the control of custom routines in LabView 2020 (NI) and a frame grabber (PCIe-1427, NI) at an acquisition rate of 100 Hz. The pupil was identified online by thresholding pixel values

and its profile was fitted with an ellipse to determine the center. The eye position was measured by computing the distance between the pupil center and the corneal reflection of a reference IR LED placed along the optical axis of the camera.

VOR gain calculation

Eye tracking data were processed in customized routines in MATLAB. VOR gain was calculated as the ratio of the average of the difference of the maximum and minimum of the eye position for each sinusoidal cycle and the amplitude of table rotation (10 degrees, 10s trial duration for all rotation frequencies). VOR gain was calculated using sinusoidal cycles that did not contain saccades. At least 20 trials were collected from each mouse.

Purkinje cell simple spikes identification

Automated spike sorting was carried out using KiloSort (https://github.com/cortex-lab/Kilosort) [91] by manual curation of the units using Phy2 (https://github.com/cortex-lab/phy). Multiple parameters were used to identify putative Purkinje cell units (Fig. 2.5). First, we only included units that exhibited spikes across at least 3 adjacent channels on the linear probe (25 μm inter-channel distance) to bias selection towards cells that have large somatodendritic area. This is thought to exclude units arising from molecular layer interneurons [92]. Second, we excluded units with refractory period violations greater than 1-2%. Simple spikes from putative Purkinje cell units were then validated using previously defined standards based on mean firing rates (> 22 Hz), median inter-spike intervals, inter-spike interval (ISI) distributions, and the coefficient of variation of the natural log of

the ISIs (Range: 0.05 to 0.4) [93]. Purkinje cell units outside of these ranges were excluded from subsequent data analysis. We also excluded complex spikes from our analysis.

Firing frequency and CV of ISI computation

All analysis was carried out via MATLAB (MathWorks) and Python on identified Purkinje cell units. The timings of each simple spike were aligned with individual trials of VOR recordings using a digital pulse triggered by a photodiode positioned on the virtual drum. Only simple spikes that occurred during the 10-second sinusoidal oscillation trials were included in subsequent analyses. To determine directional bias of the recorded PC units, we used the ratio of simple spikes frequency during clockwise (CW) and counterclockwise (CCW) head rotation in each trial (Fig. 3.3). Overall simple spike firing frequency was calculated by treating each trial (10 seconds) as a bin and dividing the total number of spikes by the duration of the trial. The firing frequency from each trial was then averaged within each experimental epoch, including pre- and post-gain down induction. The firing frequency of each trial during gain-down induction was calculated in the same way but was binned every 4 trials and normalized to the first bin to show percentage change over time. The coefficient of variation (CV) of the inter-spike intervals (ISI) was calculated on the same set of Purkinje cell simple spikes.

Ex vivo Electrophysiology:

Ex vivo cerebellar tissue preparation

Mice aged P28 through P59 were anesthetized and 250 µm-thick acute coronal slices containing the cerebellum were prepared. Slices were prepared from *Scn2a*$^{+/-}$ or wild-type littermates (genotyped by PCR). All data were acquired and analyzed blind to *Scn2a* genotype. Data were acquired from both sexes (blind to sex). Cutting solution contained (in mM): 87 NaCl, 25 $NaHCO_3$, 25 glucose, 75 sucrose, 2.5 KCl, 1.25 NaH_2PO_4, 0.5 $CaCl_2$ and 7 $MgCl_2$; bubbled with 5%CO_2/95%O_2; 4°C. Following cutting, slices were incubated in recording solution for 30 min at 33°C, then at room temperature until recording. Recordings solution contained (in mM): 125 NaCl, 2.5 KCl, 1.3 $CaCl_2$, 1 $MgCl_2$, 25 $NaHCO_3$, 1.25 NaH_2PO_4, 25 glucose; bubbled with 5%CO_2/95%O_2; 32-34°C, ~310 mOsm at ~33°C.

Ex vivo electrophysiological recordings

Cerebellar Purkinje cells and granule cells were visualized with differential interference contrast (DIC) optics for conventional visually guided whole-cell recording. For current-clamp recordings, patch electrodes (Schott 8250 glass, 7-8 MΩ tip resistance for granule cells, 3-4 MΩ tip resistance for Purkinje cells) were filled with a solution containing (in mM): 113 K-Gluconate, 9 HEPES, 4.5 $MgCl_2$, 0.1 EGTA, 14 $Tris_2$-phosphocreatine, 4 Na_2-ATP, 0.3 tris-GTP; ~290 mOsm, pH: 7.2-7.25. For voltage-clamp recordings and synaptic activity in Purkinje cells, patch electrodes (Schott 8250 glass, 3-4 MΩ tip resistance) were filled internal solution contained (in mM): 110 $CsMeSO_3$,

40 HEPES, 1 KCl, 4 NaCl, 4 Mg-ATP, 10 Na-phosphocreatine, 0.4 Na_2-GTP, 0.1 EGTA; ~290 mOsm, pH: 7.22. All data were corrected for measured junction potentials of 12 and 11 mV in K- and Cs-based internals, respectively.

Electrophysiological data were acquired using Multiclamp 700A or 700B amplifiers (Molecular Devices) via custom routines in IgorPro (Wavemetrics). For measurements of action potential waveform and fiber volleys, data were acquired at 50 kHz and filtered at 20 kHz. For all other measurements, data were acquired at 10-20 kHz and filtered at 3-10 kHz. For current-clamp recordings, pipette capacitance was compensated by 50% of the fast capacitance measured under gigaohm seal conditions in voltage-clamp prior to establishing a whole-cell configuration, and the bridge was balanced. For voltage-clamp recordings, pipette capacitance was compensated completely, and series resistance was compensated 50%.

Parallel fiber volley recordings were made from coronal slices of the medial posterior cerebellum. The recording electrode was placed ~1 mm away from a tungsten bipolar stereotrode (WE3ST30.1A10; MicroProbes for Life Science). The strength of electrical stimulation was adjusted for each recording to maintain the amplitude of the first parallel fiber volley above 1 mV. Parallel fiber volleys were evoked by field electrical stimulation in either trains of 10 at 20 ms inter-stimulus-interval or trains of 20 at 6 ms ISI. This experiment was performed in the presence of 10 μM 6,7-dinitroquinoxaline-2,3-dione (DNQX) and 25 μM picrotoxin.

In experiments measuring paired pulse ratio and synaptic plasticity, EPSCs were evoked via a bipolar glass theta electrode placed ~200 μm orthogonal and ~200 um

lateral to the recorded neuron in the molecular layer in the presence of 25 μM picrotoxin at -80 mV.

Whole-cell voltage-clamp recordings were made from the lobule 4/5 of the cerebellum. In short-term synaptic facilitation protocols, excitatory postsynaptic currents (EPSCs) were evoked by field electrical stimulation in a train of 20 at 6 ms ISI.

In high-frequency burst-based plasticity protocols, excitatory postsynaptic currents (EPSCs) were evoked with a theta stimulating electrode placed ~200 μm into the molecular layer and ~200 um lateral to the recorded Purkinje cell. After establishing a stable baseline of 5 minutes (EPSC ISI: 15 seconds) in voltage clamp, EPSPs were evoked by field electrical stimulation in a train of 10 at 6 ms ISI. Trains were repeated every 1 s for 5 minutes. Following induction, EPSC stimulation frequency was reset to 0.05 Hz, and changes in EPSC amplitudes were assessed by comparing data 25 - 30 min following induction to baseline (-5.0 - 0 min).

Statistics:

Statistical analyses were performed using IgorPro8 unless otherwise noted (Wavemetrics). No statistical tests were used to predetermine sample size, but our sample sizes are similar to those generally employed in the field. All data are presented in text as mean ± standard error (SEM), unless otherwise noted. The stated P values are the results of the non-parametric Wilcoxon rank sum test to compare values between different mice or recordings, and the non-parametric Wilcoxon signed rank test to compare values from the same recording in different experimental conditions, unless otherwise noted. Mixed-effects modeling was used to compare simple spike firing

frequency between baseline and post-induction (units nested within parent animals) using Prism. Data were corrected for multiple comparisons when necessary, using the Holm-Šídák method.

References

1. Foster, M. A textbook of physiology, book three: The central nervous system and its instruments. *MacMillan & Co Ltd* 929–930 (1897).
2. Hodgkin, A. L. & Huxley, A. F. A quantitative description of membrane current and its application to conduction and excitation in nerve. *J Physiol* (1952) doi:10.1113/jphysiol.1952.sp004764.
3. Armstrong, C. M. Na channel inactivation from open and closed states. *Proc Natl Acad Sci U S A* (2006) doi:10.1073/pnas.0607603103.
4. Hildebrand, M. E. *et al.* Identification of sodium channel isoforms that mediate action potential firing in lamina I/II spinal cord neurons. *Mol Pain* (2011) doi:10.1186/1744-8069-7-67.
5. Wang, J., Ou, S. W. & Wang, Y. J. Distribution and function of voltage-gated sodium channels in the nervous system. *Channels* Preprint at https://doi.org/10.1080/19336950.2017.1380758 (2017).
6. Kalume, F., Yu, F. H., Westenbroek, R. E., Scheuer, T. & Catterall, W. A. Reduced Sodium Current in Purkinje Neurons from NaV1.1 Mutant Mice: Implications for Ataxia in Severe Myoclonic Epilepsy in Infancy. *Journal of Neuroscience* **27**, 11065–11074 (2007).
7. Whitaker, W. R. J. *et al.* Distribution of voltage-gated sodium channel α-subunit and β-subunit mRNAs in human hippocampal formation, cortex, and cerebellum. *Journal of Comparative Neurology* (2000) doi:10.1002/(SICI)1096-9861(20000619)422:1<123::AID-CNE8>3.0.CO;2-X.

8. Martínez-Hernández, J. *et al.* Polarised localisation of the voltage-gated sodium channel Na v1.2 in cerebellar granule cells. *Cerebellum* (2013) doi:10.1007/s12311-012-0387-1.

9. Spratt, P. W. E. *et al.* The Autism-Associated Gene Scn2a Contributes to Dendritic Excitability and Synaptic Function in the Prefrontal Cortex. *Neuron* (2019) doi:10.1016/j.neuron.2019.05.037.

10. Lorincz, A. & Nusser, Z. Molecular Identity of Dendritic Voltage-Gated Sodium Channels. *Science (1979)* **328**, 906–909 (2010).

11. Chadderton, P., Margie, T. W. & Häusser, M. Integration of quanta in cerebellar granule cells during sensory processing. *Nature* **428**, 856–860 (2004).

12. Jörntell, H. & Ekerot, C. F. Properties of somatosensory synaptic integration in cerebellar granule cells in vivo. *Journal of Neuroscience* (2006) doi:10.1523/JNEUROSCI.2939-06.2006.

13. van Beugen, B. J., Gao, Z., Boele, H. J., Hoebeek, F. & De Zeeuw, C. I. High frequency burst firing of granule cells ensures transmission at the parallel fiber to purkinje cell synapse at the cost of temporal coding. *Front Neural Circuits* **7**, 1–12 (2013).

14. Park, D. & Dunlap, K. Dynamic regulation of calcium influx by G-proteins, action potential waveform, and neuronal firing frequency. *J Neurosci* **18**, 6757–6766 (1998).

15. Borst, J. G. G. & Sakmann, B. Effect of changes in action potential shape on calcium currents and transmitter release in a calyx-type synapse of the rat

auditory brainstem. in *Philosophical Transactions of the Royal Society B: Biological Sciences* (1999). doi:10.1098/rstb.1999.0386.

16. Brose, N., Petrenko, A. G., Sudhof, T. C. & Jahn, R. Synaptotagmin: A calcium sensor on the synaptic vesicle surface. *Science (1979)* (1992) doi:10.1126/science.1589771.
17. Dodge, F. A. & Rahamimoff, R. Co-operative action of calcium ions in transmitter release at the neuromuscular junction. *J Physiol* (1967) doi:10.1113/jphysiol.1967.sp008367.
18. Meldrum, B. S. Glutamate as a neurotransmitter in the brain: Review of physiology and pathology. in *Journal of Nutrition* (2000). doi:10.1093/jn/130.4.1007s.
19. Stanton, P. K. LTD, LTP, and the sliding threshold for long-term synaptic plasticity. *Hippocampus* (1996) doi:10.1002/(SICI)1098-1063(1996)6:1<35::AID-HIPO7>3.0.CO;2-6.
20. Salin, P. A., Malenka, R. C. & Nicoll, R. A. Cyclic AMP mediates a presynaptic form of LTP at cerebellar parallel fiber synapses. *Neuron* **16**, 797–803 (1996).
21. Qiu, D. L. & Knöpfel, T. Presynaptically expressed long-term depression at cerebellar parallel fiber synapses. *Pflugers Arch* (2009) doi:10.1007/s00424-008-0555-9.
22. Van Beugen, B. J., Nagaraja, R. Y. & Hansel, C. Climbing fiber-evoked endocannabinoid signaling heterosynaptically suppresses presynaptic cerebellar long-term potentiation. *Journal of Neuroscience* (2006) doi:10.1523/JNEUROSCI.0805-06.2006.

23. Lev-Ram, V., Wong, S. T., Storm, D. R. & Tsien, R. Y. A new form of cerebellar long-term potentiation is postsynaptic and depends on nitric oxide but not cAMP. *Proc Natl Acad Sci U S A* (2002) doi:10.1073/pnas.122206399.

24. Lev-Ram, V., Mehta, S. B., Kleinfeld, D. & Tsien, R. Y. Reversing cerebellar long-term depression. *Proc Natl Acad Sci U S A* (2003) doi:10.1073/pnas.2636935100.

25. Ito, M. & Kano, M. Long-lasting depression of parallel fiber-Purkinje cell transmission induced by conjunctive stimulation of parallel fibers and climbing fibers in the cerebellar cortex. *Neurosci Lett* (1982) doi:10.1016/0304-3940(82)90380-9.

26. Storm, D. R., Hansel, C., Hacker, B., Parent, A. & Linden, D. J. Impaired cerebellar long-term potentiation in type I adenylyl cyclase mutant mice. *Neuron* (1998) doi:10.1016/S0896-6273(00)80500-0.

27. Brown, S. P., Safo, P. K. & Regehr, W. G. Endocannabinoids Inhibit Transmission at Granule Cell to Purkinje Cell Synapses by Modulating Three Types of Presynaptic Calcium Channels. *Journal of Neuroscience* **24**, (2004).

28. Brown, S. P., Brenowitz, S. D. & Regehr, W. G. Brief presynaptic bursts evoke synapse-specific retrograde inhibition mediated by endogenous cannabinoids. *Nat Neurosci* (2003) doi:10.1038/nn1126.

29. De Zeeuw, C. I. & Ten Brinke, M. M. Motor learning and the cerebellum. *Cold Spring Harb Perspect Biol* **7**, 1–20 (2015).

30. Koziol, L. F. *et al.* Consensus paper: The cerebellum's role in movement and cognition. *Cerebellum* Preprint at https://doi.org/10.1007/s12311-013-0511-x (2014).

31. Schmahmann, J. D. The cerebellum and cognition. *Neuroscience Letters* Preprint at https://doi.org/10.1016/j.neulet.2018.07.005 (2019).
32. Oscarrson, O. Neurobiology of cerebellar evolution and development . Llinás, R. (ed.). Proceedings of the first international symposium of the institute for biomedical research: Ama education research foundation. American medical association: Chicago, 1969, 941 pages . *J Neurobiol* (1971) doi:10.1002/neu.480020405.
33. Eccles, J. C., Ito, M. & Szentágothai, J. *The Cerebellum as a Neuronal Machine*. *The Cerebellum as a Neuronal Machine* (1967). doi:10.1007/978-3-662-13147-3.
34. Galliano, E. *et al.* Silencing the Majority of Cerebellar Granule Cells Uncovers Their Essential Role in Motor Learning and Consolidation. *Cell Rep* (2013) doi:10.1016/j.celrep.2013.03.023.
35. Ito, M. Cerebellar Control of the Vestibulo-Ocular Reflex–Around the Flocculus Hypothesis. *Annu Rev Neurosci* (1982) doi:10.1146/annurev.ne.05.030182.001423.
36. Crawford, J. D. & Vilis, T. Axes of eye rotation and Listing's law during rotations of the head. *J Neurophysiol* (1991) doi:10.1152/jn.1991.65.3.407.
37. Voges, K., Wu, B., Post, L., Schonewille, M. & De Zeeuw, C. I. Mechanisms underlying vestibulo-cerebellar motor learning in mice depend on movement direction. *Journal of Physiology* (2017) doi:10.1113/JP274346.
38. De Zeeuw, C. I. *et al.* Expression of a protein kinase C inhibitor in purkinje cells blocks cerebellar LTD and adaptation of the vestibulo-ocular reflex. *Neuron* (1998) doi:10.1016/S0896-6273(00)80990-3.

39. Hansel, C. *et al.* αCaMKII Is Essential for Cerebellar LTD and Motor Learning. *Neuron* (2006) doi:10.1016/j.neuron.2006.08.013.

40. Boyden, E. S. *et al.* Selective Engagement of Plasticity Mechanisms for Motor Memory Storage. *Neuron* (2006) doi:10.1016/j.neuron.2006.08.026.

41. Feil, R. *et al.* Impairment of LTD and cerebellar learning by Purkinje cell-specific ablation of cGMP-dependent protein kinase I. *Journal of Cell Biology* (2003) doi:10.1083/jcb.200306148.

42. Sanders, S. J. *et al.* Progress in Understanding and Treating SCN2A-Mediated Disorders. *Trends in Neurosciences* Preprint at https://doi.org/10.1016/j.tins.2018.03.011 (2018).

43. Satterstrom, F. K. *et al.* Large-Scale Exome Sequencing Study Implicates Both Developmental and Functional Changes in the Neurobiology of Autism. *Cell* (2020) doi:10.1016/j.cell.2019.12.036.

44. Sanders, S. J. *et al.* De novo mutations revealed by whole-exome sequencing are strongly associated with autism. *Nature* (2012) doi:10.1038/nature10945.

45. Fu, J. M. *et al.* Rare coding variation provides insight into the genetic architecture and phenotypic context of autism. *Nat Genet* (2022) doi:10.1038/s41588-022-01104-0.

46. Ben-Shalom, R. *et al.* Opposing Effects on Na V 1.2 Function Underlie Differences Between SCN2A Variants Observed in Individuals With Autism Spectrum Disorder or Infantile Seizures. *Biol Psychiatry* **82**, 224–232 (2017).

47. Hu, W. *et al.* Distinct contributions of Nav1.6 and Nav1.2 in action potential initiation and backpropagation. *Nat Neurosci* (2009) doi:10.1038/nn.2359.

48. Devlin, B. *et al.* Patterns and rates of exonic de novo mutations in autism spectrum disorders. *Nature* Preprint at https://doi.org/10.1038/nature11011 (2012).

49. Tavassoli, T. *et al.* De novo SCN2A splice site mutation in a boy with Autism spectrum disorder. *BMC Med Genet* (2014) doi:10.1186/1471-2350-15-35.

50. Jiang, Y. H. *et al.* Detection of clinically relevant genetic variants in autism spectrum disorder by whole-genome sequencing. *Am J Hum Genet* (2013) doi:10.1016/j.ajhg.2013.06.012.

51. Hoischen, A., Krumm, N. & Eichler, E. E. Prioritization of neurodevelopmental disease genes by discovery of new mutations. *Nature Neuroscience* Preprint at https://doi.org/10.1038/nn.3703 (2014).

52. Johnson, M. R. *et al.* Systems genetics identifies a convergent gene network for cognition and neurodevelopmental disease. *Nat Neurosci* (2016) doi:10.1038/nn.4205.

53. Li, J. *et al.* Genes with de novo mutations are shared by four neuropsychiatric disorders discovered from NPdenovo database. *Mol Psychiatry* (2016) doi:10.1038/mp.2015.40.

54. Bender, K. J. & Trussell, L. O. The Physiology of the Axon Initial Segment. *Annu Rev Neurosci* (2012) doi:10.1146/annurev-neuro-062111-150339.

55. Marko, M. K. *et al.* Behavioural and neural basis of anomalous motor learning in children with autism. *Brain* (2015) doi:10.1093/brain/awu394.

56. Holmes, G. The symptoms of acute cerebellar injuries due to gunshot injuries. *Brain* (1917) doi:10.1093/brain/40.4.461.

57. Schmahmann, J. D., Weilburg, J. B. & Sherman, J. C. The neuropsychiatry of the cerebellum - Insights from the clinic. *Cerebellum* Preprint at https://doi.org/10.1080/14734220701490995 (2007).

58. Ritvo, E. R. *et al.* Lower Purkinje cell counts in the cerebella of four autistic subjects: Initial findings of the UCLA-NSAC autopsy research report. *American Journal of Psychiatry* (1986) doi:10.1176/ajp.143.7.862.

59. Bailey, A. *et al.* A clinicopathological study of autism. *Brain* (1998) doi:10.1093/brain/121.5.889.

60. Fatemi, S. H. *et al.* Purkinje cell size is reduced in cerebellum of patients with autism. *Cell Mol Neurobiol* (2002) doi:10.1023/A:1019861721160.

61. Kemper, T. L. & Bauman, M. L. Neuropathology of infantile autism. *Mol Psychiatry* (2002) doi:10.1038/sj.mp.4001165.

62. Bodranghien, F. *et al.* Consensus Paper: Revisiting the Symptoms and Signs of Cerebellar Syndrome. *Cerebellum* Preprint at https://doi.org/10.1007/s12311-015-0687-3 (2016).

63. Takarae, Y., Minshew, N. J., Luna, B., Krisky, C. M. & Sweeney, J. A. Pursuit eye movement deficits in autism. *Brain* (2004) doi:10.1093/brain/awh307.

64. Gutierrez-Castellanos, N. *et al.* Motor Learning Requires Purkinje Cell Synaptic Potentiation through Activation of AMPA-Receptor Subunit GluA3. *Neuron* (2017) doi:10.1016/j.neuron.2016.11.046.

65. Ito, M. Cerebellar Control of the Vestibulo-Ocular Reflex--Around the Flocculus Hypothesis. *Annu Rev Neurosci* (1982) doi:10.1146/annurev.ne.05.030182.001423.

66. Ulbricht, W. Sodium channel inactivation: Molecular determinants and modulation. *Physiological Reviews* Preprint at https://doi.org/10.1152/physrev.00024.2004 (2005).

67. JENKINSON, D. H. The nature of the antagonism between calcium and magnesium ions at the neuromuscular junction. *J Physiol* (1957) doi:10.1113/jphysiol.1957.sp005860.

68. Katz, B. & Miledi, R. The role of calcium in neuromuscular facilitation. *J Physiol* (1968) doi:10.1113/jphysiol.1968.sp008469.

69. Bouvier, G. *et al.* Burst-Dependent Bidirectional Plasticity in the Cerebellum Is Driven by Presynaptic NMDA Receptors. *Cell Rep* (2016) doi:10.1016/j.celrep.2016.03.004.

70. Prakriya, M. & Mennerick, S. Selective depression of low-release probability excitatory synapses by sodium channel blockers. *Neuron* (2000) doi:10.1016/S0896-6273(00)81203-9.

71. Cho, I. H., Panzera, L. C., Chin, M. & Hoppa, M. B. Sodium channel β2 subunits prevent action potential propagation failures at axonal branch points. *Journal of Neuroscience* (2017) doi:10.1523/JNEUROSCI.0891-17.2017.

72. De Col, R., Messlinger, K. & Carr, R. W. Conduction velocity is regulated by sodium channel inactivation in unmyelinated axons innervating the rat cranial meninges. *Journal of Physiology* (2008) doi:10.1113/jphysiol.2007.145383.

73. Ogiwara, I. *et al.* Nav1.2 haplodeficiency in excitatory neurons causes absence-like seizures in mice. *Commun Biol* (2018) doi:10.1038/s42003-018-0099-2.

74. Badura, A. *et al.* Normal cognitive and social development require posterior cerebellar activity. *Elife* **7**, (2018).

75. Carta, I., Chen, C. H., Schott, A. L., Dorizan, S. & Khodakhah, K. Cerebellar modulation of the reward circuitry and social behavior. *Science (1979)* (2019) doi:10.1126/science.aav0581.

76. Carta, I., Chen, C. H., Schott, A. L., Dorizan, S. & Khodakhah, K. Cerebellar modulation of the reward circuitry and social behavior. *Science (1979)* (2019) doi:10.1126/science.aav0581.

77. Powell, K., Mathy, A., Duguid, I. & Häusser, M. Synaptic representation of locomotion in single cerebellar granule cells. *Elife* (2015) doi:10.7554/eLife.07290.

78. Ishikawa, T., Shimuta, M. & Häuser, M. Multimodal sensory integration in single cerebellar granule cells in vivo. *Elife* (2015) doi:10.7554/eLife.12916.

79. Broussard, D. M., Titley, H. K., Antflick, J. & Hampson, D. R. Motor learning in the VOR: The cerebellar component. in *Experimental Brain Research* (2011). doi:10.1007/s00221-011-2589-z.

80. Beh, S. C., Frohman, T. C. & Frohman, E. M. Cerebellar control of eye movements. *Journal of Neuro-Ophthalmology* Preprint at https://doi.org/10.1097/WNO.0000000000000456 (2017).

81. Marr, D. A theory of cerebellar cortex. *J Physiol* (1969) doi:10.1113/jphysiol.1969.sp008820.

82. Tatsukawa, T. *et al.* Scn2a haploinsufficient mice display a spectrum of phenotypes affecting anxiety, sociability, memory flexibility and ampakine CX516 rescues their hyperactivity. *Mol Autism* (2019) doi:10.1186/s13229-019-0265-5.

83. Shin, W. *et al.* Scn2a haploinsufficiency in mice suppresses hippocampal neuronal excitability, excitatory synaptic drive, and long-term potentiation, and spatial learning and memory. *Front Mol Neurosci* (2019) doi:10.3389/fnmol.2019.00145.

84. Tamura, S. *et al.* CRISPR activation rescues abnormalities in SCN2A haploinsufficiency-associated autism spectrum disorder. *bioRxiv* 2022.03.30.486483 (2022) doi:10.1101/2022.03.30.486483.

85. Matharu, N. *et al.* CRISPR-mediated activation of a promoter or enhancer rescues obesity caused by haploinsufficiency. *Science (1979)* (2019) doi:10.1126/science.aau0629.

86. Yardeni, T., Eckhaus, M., Morris, H. D., Huizing, M. & Hoogstraten-Miller, S. Retro-orbital injections in mice. *Lab Animal* Preprint at https://doi.org/10.1038/laban0511-155 (2011).

87. Mathis, A. *et al.* DeepLabCut: markerless pose estimation of user-defined body parts with deep learning. *Nat Neurosci* (2018) doi:10.1038/s41593-018-0209-y.

88. Bahn, S., Jones, A. & Wisden, W. Directing gene expression to cerebellar granule cells using γ-aminobutyric acid type A receptor α6 subunit transgenes. *Proc Natl Acad Sci U S A* (1997) doi:10.1073/pnas.94.17.9417.

89. Planells-Cases, R. *et al.* Neuronal death and perinatal lethality in voltage-gated sodium channel α(II)-deficient mice. *Biophys J* (2000) doi:10.1016/S0006-3495(00)76829-9.

90. Liu, B. H., Huberman, A. D. & Scanziani, M. Cortico-fugal output from visual cortex promotes plasticity of innate motor behaviour. *Nature* (2016) doi:10.1038/nature19818.

91. Pachitariu, M., Sridhar, S. & Stringer, C. Solving the spike sorting problem with Kilosort. *bioRxiv* 2023.01.07.523036 (2023) doi:10.1101/2023.01.07.523036.

92. Gaffield, M. A., Sauerbrei, B. A. & Christie, J. M. Cerebellum encodes and influences the initiation, performance, and termination of discontinuous movements in mice. *Elife* **11**, e71464 (2022).

93. van Dijck, G. *et al.* Probabilistic Identification of Cerebellar Cortical Neurones across Species. *PLoS One* (2013) doi:10.1371/journal.pone.0057669.

Publishing Agreement

It is the policy of the University to encourage open access and broad distribution of all theses, dissertations, and manuscripts. The Graduate Division will facilitate the distribution of UCSF theses, dissertations, and manuscripts to the UCSF Library for open access and distribution. UCSF will make such theses, dissertations, and manuscripts accessible to the public and will take reasonable steps to preserve these works in perpetuity.

I hereby grant the non-exclusive, perpetual right to The Regents of the University of California to reproduce, publicly display, distribute, preserve, and publish copies of my thesis, dissertation, or manuscript in any form or media, now existing or later derived, including access online for teaching, research, and public service purposes.

DocuSigned by:
Chenyu Wang
35933ABDA10849A...
Author Signature

5/18/2023
Date